JGR Planets

RESEARCH ARTICLE
10.1029/2024JE008862

The Sporadic Fluvial Regime of Pliva Vallis, the Outlet Valley of Jezero Crater Lake, Mars

J. Villette[1], N. Mangold[1], E. S. Kite[2], S. J. Conway[1], and L. Le Deit[1]

[1]Nantes Université, Univ Angers, Le Mans Université, CNRS, Laboratoire de Planétologie et Géosciences, LPG UMR 6112, Nantes, France, [2]Department of the Geophysical Sciences, The University of Chicago, Chicago, IL, USA

Abstract In situ and orbital observations have suggested that Jezero crater (field site for the Mars 2020 Perseverance rover) once hosted a paleolake fed by two inlet valleys. An outlet valley, Pliva Vallis, is present on the eastern rim of the crater and raises the question of whether the lake system operated as an open basin or as a closed basin system with one or more overflow events. To tackle this uncertainty, we present a detailed morphological study of Pliva Vallis, using digital elevation models and imagery. The atypical morphology of the valley, including reincised fluvial layered deposits, a perched valley, and bedrock incision terraces, led us to interpret that Pliva Vallis was formed by discontinuous and episodic flows rather than from a steady outlet river. These observations allowed us to infer at least four main breach episodes and propose a new scenario for the evolution of the lake system over time. We give a minimum estimate of the duration of these overflow events using a 0-D model, simulating a valley formation by breach erosion and lake overflow. Modeling results suggest that each flood event causing a part of the incision of the outlet valley would not have lasted for more than a few weeks, and some may have lasted only a few days. These time scales are consistent with our morphological interpretation that the outlet valley was carved by discontinuous and temporary flows. In this scenario, Jezero lake was predominantly a closed basin, spilling over episodically in at least four breach events.

Plain Language Summary Mars had lakes and rivers in the past. Jezero crater, an ancient lake that is now dry, has two inlet valleys that fed water into the lake, and a single outlet valley, Pliva Vallis. We conducted a detailed study of Pliva Vallis to understand the nature of the lake system: was Jezero crater lake an open basin, which is a lake with rivers leading into and out of it, or a closed basin, with only rivers leading into it, or episodically open? To answer this question, we used data from Martian orbital probes. By examining the shape of the valley, we noticed that Pliva Vallis was not like valleys carved by continuous rivers on Earth and propose instead that the valley was carved by at least four episodes of lake overflow. To give a minimum estimate of the duration of these events, we use a numerical model to simulate the overflow of a lake and the incision of a valley. Modeling suggests that the four (or more) episodes identified each incised part of the valley and that each episode lasted a few weeks at maximum.

Key Points:

- We present a new scenario for the formation of Pliva Vallis, the outlet valley of the Jezero crater lake
- Observations point to episodic incision of Pliva Vallis in ≥4 lake Jezero overflow events
- Modeling results suggest that each incision lasted at most a few weeks

Supporting Information:

Supporting Information may be found in the online version of this article.

Correspondence to:

J. Villette,
justine.villette@univ-nantes.fr

Citation:

Villette, J., Mangold, N., Kite, E. S., Conway, S. J., & Le Deit, L. (2025). The sporadic fluvial regime of Pliva Vallis, the outlet valley of Jezero crater lake, Mars. *Journal of Geophysical Research: Planets*, *130*, e2024JE008862. https://doi.org/10.1029/2024JE008862

Received 14 NOV 2024
Accepted 23 APR 2025

Author Contributions:

Conceptualization: J. Villette, N. Mangold, E. S. Kite, S. J. Conway, L. Le Deit
Formal analysis: J. Villette
Investigation: J. Villette, N. Mangold
Methodology: J. Villette, N. Mangold, E. S. Kite, S. J. Conway, L. Le Deit
Project administration: J. Villette, N. Mangold
Resources: N. Mangold, E. S. Kite
Supervision: J. Villette, N. Mangold, S. J. Conway, L. Le Deit
Validation: J. Villette, N. Mangold, E. S. Kite, S. J. Conway, L. Le Deit
Visualization: J. Villette, N. Mangold
Writing – original draft: J. Villette, N. Mangold
Writing – review & editing: J. Villette, N. Mangold, E. S. Kite, S. J. Conway, L. Le Deit

1. Introduction

Orbital observations by the Mariner 9 and Viking probes revealed evidence for past surface water activity on Mars, such as valley networks (Masursky, 1973; Carr et al., 1976; Pieri, 1980; Carr, 1987; Howard et al., 2005; Irwin, Craddock, & Howard, 2005; Irwin, Howard, et al., 2005), and paleolakes (Cabrol & Grin, 1999, 2001, 2010; De Hon, 1992; Goldspiel & Squyres, 1991; Irwin, Howard, et al., 2005; Wharton et al., 1995). At present, >100 paleolakes have been identified on Mars, often classified as open and closed basin lakes (Cabrol & Grin, 1999; Fassett & Head, 2008a; Goudge et al., 2012; Goudge, Aureli et al., 2015). An open basin is a basin with an active outlet valley, whereas in a closed basin, the water does not flow through an outlet valley. Most are dated to the Late Noachian and/or Early Hesperian (Ehlmann et al., 2008; Fassett & Head, 2005, 2008b; Hoke & Hynek, 2009; Irwin, Howard, et al., 2005; Mangold et al., 2012, 2020), although some are younger (Kite & Noblet, 2022).

Jezero crater, which is the landing site for the Perseverance rover sent as part of the Mars 2020 mission, is an extensively studied palaeolake. Jezero crater, 45 km in diameter, is located west of Isidis Planitia (Figure 1a) in the northern hemisphere (18.4°N, 77.5°E). Two inlet valleys, Neretva Vallis and Sava Vallis, each with a depositional fan, and an outlet valley at higher elevation than the fans, Pliva Vallis (Figure 1b), attest to the presence of a past lake (Fassett & Head, 2005; Goudge, Mustard, et al., 2015; Schon et al., 2012). In addition to

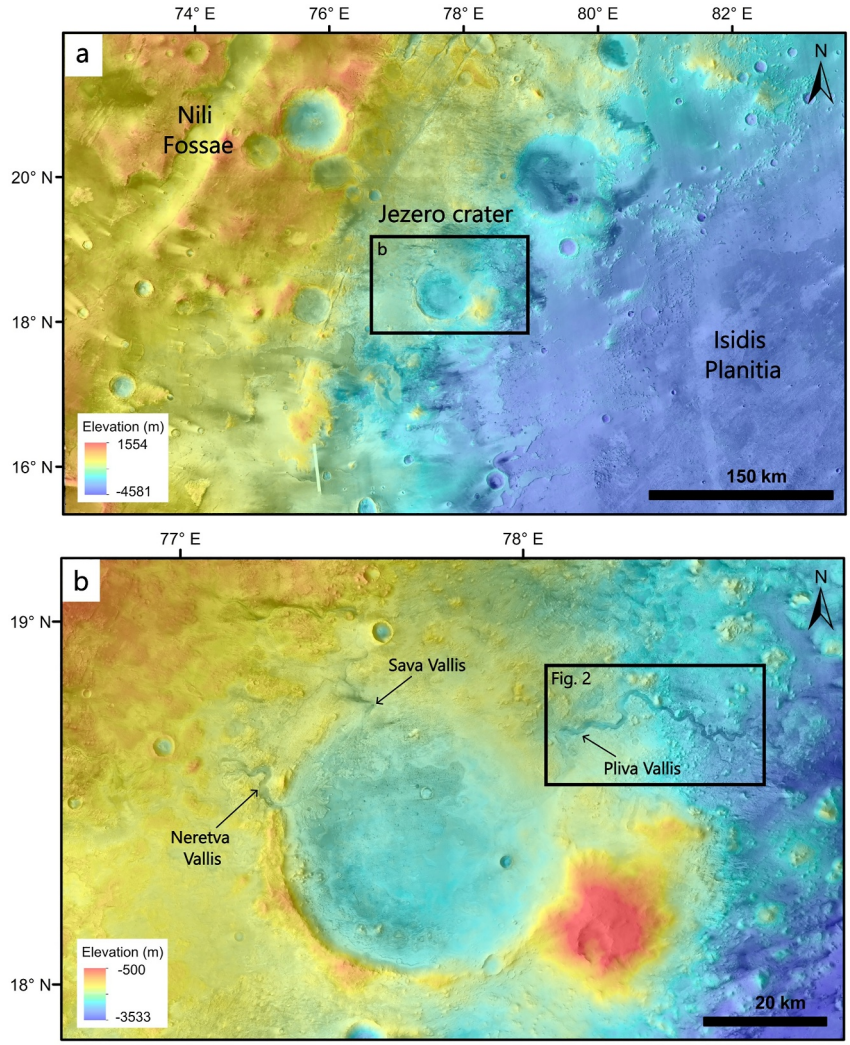

Figure 1. (a) Location map of Jezero crater (18.4°N, 77.5°E), west of Isidis Planitia and east of Nili Fossae. (b) Detailed view of Jezero crater and location of the two inlet valleys (Neretva Vallis and Sava Vallis) and the outlet valley (Pliva Vallis). MOLA DTM overlain on a mosaic of CTX images (CTX_V01_E72_N20_Mosaic, CTX_V01_E76_N20_Mosaic, CTX_V01_E80_N20_Mosaic, CTX_V01_E72_N16_Mosaic, CTX_V01_E76_N16_Mosaic, CTX_V01_E80_N16_Mosaic, CTX_V01_E72_N12_Mosaic, CTX_V01_E76_N12_Mosaic, CTX_V01_E80_N12_Mosaic).

geomorphological evidence, orbital spectra show the presence of carbonates and phyllosilicate minerals in the region of Nili Fossae upstream (Ehlmann et al., 2008; Mangold et al., 2007; Mustard et al., 2007, 2009; Poulet et al., 2005) and in Jezero crater (Ehlmann et al., 2008; Goudge et al., 2012, Goudge, Mustard, et al., 2015; Horgan et al., 2020; Tarnas et al., 2019). These detections confirm the past circulation of liquid water in the Jezero crater region. Further, rover observations of inclined beds interpreted as delta foresets on the western fan confirm that it is a delta (Mangold et al., 2021) recording a crater lake. Thus, the Jezero crater lake is a priority for in situ study and potential sample return (McLennan et al., 2012; Salvatore et al., 2018).

However, the evolution and timing of the Jezero crater lake is still debated. Early work suggested that Jezero was an open lake basin and the outlet valley was a continuous steady river (Fassett & Head, 2005; Goudge et al., 2012; Goudge, Mustard, et al., 2015; Schon et al., 2012). However, in situ data showed that much of the delta formed when the lake level was below that of the breach to the outlet, calling into question the open-basin hypothesis (Caravaca et al., 2024; Mangold et al., 2021, 2024). Although erosion of the delta is not negligible, there is no clear evidence of major erosion in the upper part of the delta, whose altitude coincides with the altitude of Neretva Vallis at the entrance to the lake. The understanding of the nature (open or closed basin) of the Jezero crater lake is

fundamental to understanding the evolution of the lake system over time, the water chemistry, and the habitability of the lake. Hence, a better understanding of the outlet is needed.

In this paper, we conduct a complete morphological study of Pliva Vallis, the outlet valley of the Jezero crater lake, and propose a scenario for its evolution over time. Based on this scenario, we use a model to estimate the minimum duration of the outlet valley activity. The results provide new insight into the evolution of the Jezero crater lake system.

2. Data Sets

In this study, we used data acquired from the Mars Reconnaissance Orbiter (MRO, Zurek & Smrekar, 2007).

We used orbital visible images obtained from the Context Camera (CTX, Malin et al., 2007) with a spatial resolution around 5 m/pixel. We used version 1 of the CTX global mosaic (tile CTX_V01_E076_N16_Mosaic) (Dickson et al., 2018, 2024), which covers the Jezero crater region, the two inlet valleys Neretva Vallis and Sava Vallis, and the outlet valley Pliva Vallis (Figure 1b).

We also used visible images acquired from the High Resolution Imaging Science Experiment Camera (HiRISE, McEwen et al., 2007) with a spatial resolution of 0.25–1.3 m/pixel. These data give us a precise view of the outlet valley, its geometry and the deposits in the valley.

For both CTX and HiRISE data, DTMs are produced by MarsSI (Mars System of Information) from stereo image pairs using the NASA Ames stereo pipeline. The DTMs have a spatial resolution of 12 m/pixel and 1 m/pixel and a vertical precision of ∼5 m and <1 m for CTX and HiRISE, respectively (Kirk et al., 2021; Quantin-Nataf et al., 2018; Volat et al., 2022).

The HiRISE and CTX images and DTMs were then added to ArcGIS (version 10.8.1), a Geographic Information System (GIS), to visualize the data. The projection used in this project is a sinusoidal projection centered on Jezero crater (18.4°N, 77.5°E) to avoid distortion in length measurements in our study region. All the figures presented here, containing images of the region and topographical data, were produced using this GIS.

3. Results of Morphological Observations in Pliva Vallis

3.1. General Characteristics

An overview of Pliva Vallis, the outlet valley of the Jezero crater lake, is shown in Figure 2. The valley, 50 km long, is on the eastern side of Jezero crater, and runs from west to east. The valley disappears into the plains without displaying any depositional fan. The valley is moderately sinuous (sinuosity index of 1.47, calculated as the ratio between the length along the valley floor and the straight-line distance from the breach to the end of the valley), where the valley's sinuosity becomes less pronounced from upstream to downstream. In contrast, a meandering valley has relatively regular and a more pronounced sinuosity over its entire length. The valley lacks tributaries showing that only the water that flowed across Jezero's rim carved it, but has a possible distributary channel that is presented in Section 3.3.3.

At Jezero's rim, the outlet valley has incised deeply (up to 250 m) into bedrock, marked by impact craters and hills. Spectral data from orbit show that the unit incised by Pliva Vallis is an olivine-rich regional unit that has been suggested to have been substantially scoured by wind (Farley et al., 2022; Goudge, Mustard, et al., 2015; Kremer et al., 2019; Mandon et al., 2020; Mangold et al., 2007; Mustard et al., 2007, 2009).

3.2. Landforms in Pliva Vallis

3.2.1. Rock Exposures on Pliva Vallis

Parts of the Pliva Vallis floor are covered by aeolian dunes, but when absent, we observe layered deposits and bedrock outcrops that are described below from upstream to downstream. The first set of layered deposits is located just after the first bend in the valley (Figure 2). It is defined by a topographical step with a flat top on the inner edge of the valley (Figure 3a). The western part of this deposit is ∼600 m long, ∼110 m wide, 30 m high and is composed of <10 m thick, boulder-bearing beds. The eastern part of this deposit is defined by the resistant strata indicated by the white arrows in Figure 3a. The second deposit identified is >20 km downstream on the valley

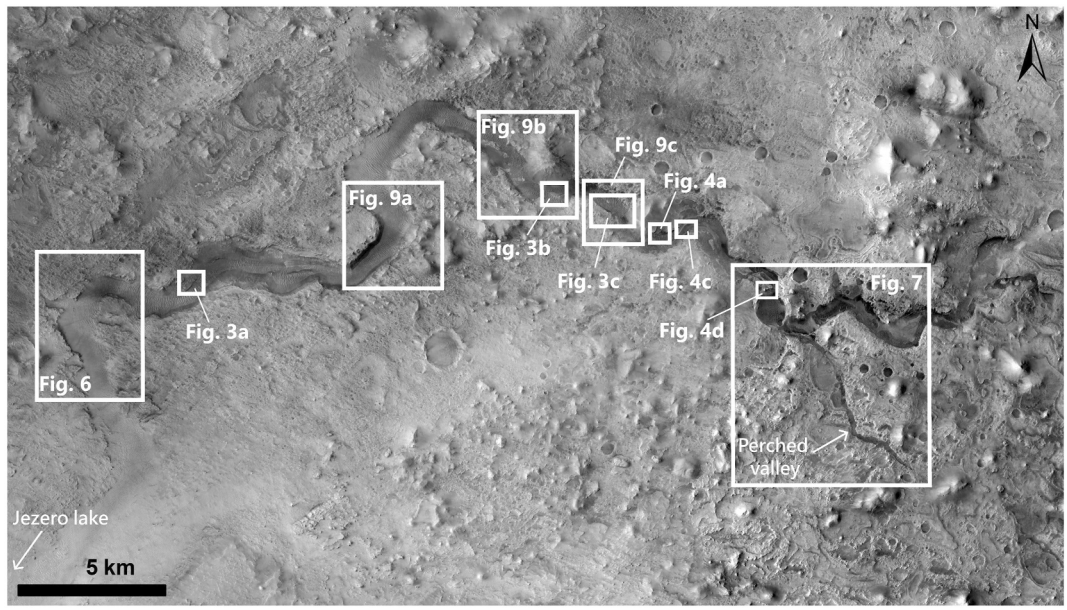

Figure 2. Part of the CTX image mosaic tile (MurrayLab_CTX_V01_E76_N16_Mosaic) showing an overview of Pliva Vallis, the outlet valley in Jezero crater. The white boxes show the location of the figures presented in this paper.

floor (Figures 2 and 3b), and is elongated (540 m long and 170 m wide) with faint layering and a fractured appearance.

Further downstream, we identified three outcrops on the valley floor (Figures 2 and 3c), partly covered by modern dunes. Figure 3d is a close-up of the largest deposit. It is ∼320 m long and 100 m wide. These outcrops have a different texture compared to the outcrops described previously with more massive appearance and rougher surfaces.

Further downstream, we identified a set of layered deposits at the foot of the northern wall of the outlet valley. This set is ∼50 m high and composed of alternating beds with varying resistance to erosion and a few meters of maximum thickness (Figures 2 and 4a). The most resistant deposits are made up of aligned boulders (Figure 4b, white arrows) located between two thin beds (black arrows). The boulder-bearing strata are composed of boulders with a maximum size of 2 m. The lateral continuity of the beds indicates a well-stratified sedimentary deposit.

Close to this outcrop sits another valley-floor deposit (Figures 2 and 4c). This is an elongated deposit, ∼740 m long, curving to follow the outlet valley. The grains are too small to be visible in the HiRISE image. Meter-sized boulders are embedded in the deposit but without any visible alignment. The final layered deposit located downstream (Figures 2 and 4d) also contains isolated meter-scale boulders locally aligned along strata (white arrows).

Notably, no visible inner channel is observed on the valley floor. While aeolian dunes cover part of the valley floor, we still observe several deposits on the valley floor, so the inner channels (had they formed) should be visible.

3.2.2. Interpretation

The layered valley-floor deposits all have the same organization of meter-scale strata and a texture with a varying abundance of boulder-bearing strata. We interpret them as sediments deposited during the fluvial activity of Pliva Vallis which were then exhumed by erosion; that is, depositional terraces. The presence of boulders embedded in all these deposits rules out aeolian transport. The texture of these deposits (boulder-bearing bedded sediments) contrasts with bedrock exposed by valley incision (rougher, without bedding), so these are deposits not erosional remnants of the surrounding bedrock.

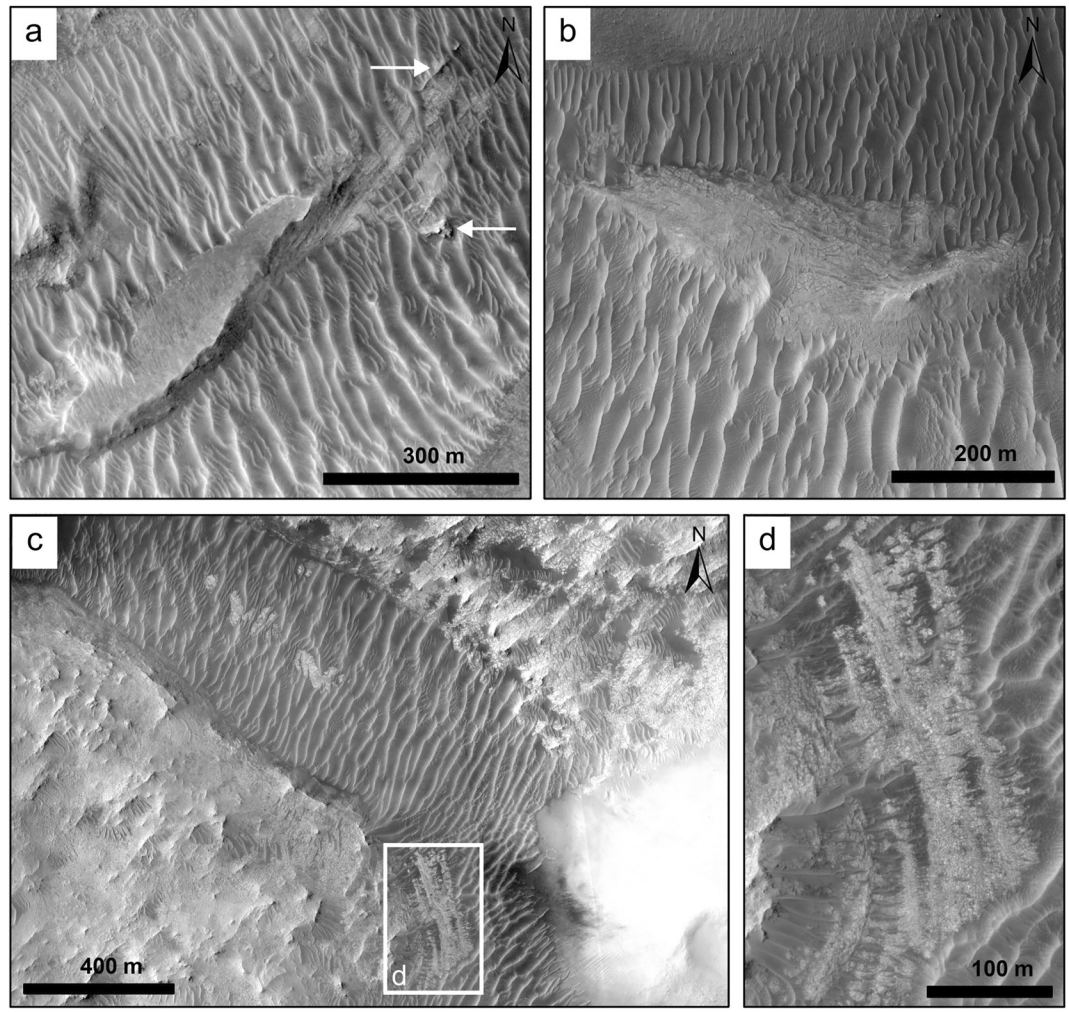

Figure 3. HiRISE images (ESP_033717_1990_RED and ESP_069653_1990_RED) of layered deposits and outcrops on the valley floor and walls. (a) Fine-grained deposit forming a small topographic step on the wall of the valley with some boulder-rich strata indicated by the white arrows. (b) Elongated and fractured deposits on the valley floor. (c) Three outcrops of bedrock on the valley floor covered by aeolian dunes. (d) Close-up view of one of the largest bedrock outcrop in Figure 3c showing details of the texture.

Here, we assume that the fluvial terrace explanation is correct because it is the only hypothesis that can explain all our observations. We suggest that the alternation between fine grained deposits and aligned boulders reflects changing flow energy over time and space: stronger flows can transport large grains (such as boulders), and weak flows can only transport fine particles (e.g., Figures 4a and 4b).

The outcrops seen in Figures 3c and 3d are different from the layered deposits. Their rougher texture and fractured appearance seem similar to the bedrock observed on the plateau on either side of the valley. The presence of outcropping bedrock on the valley floor suggests at least a low level of aeolian infilling and some erosion to expose them.

Some of these deposits appear in the form of depositional terraces, that is, river deposits cut by subsequent phases of flow (Figures 3a, 4a, and 4b). Other deposits are elongated and follow the flow path in the valley (Figure 4c). In this case, we infer that these deposits were initially deposited on the valley floor and sculpted by subsequent fluvial erosion.

Many other deposits are also observed downstream of the valley and are interpreted as stratified sedimentary deposits resulting from the fluvial activity of Pliva Vallis (Figure S1 in Supporting Information S1).

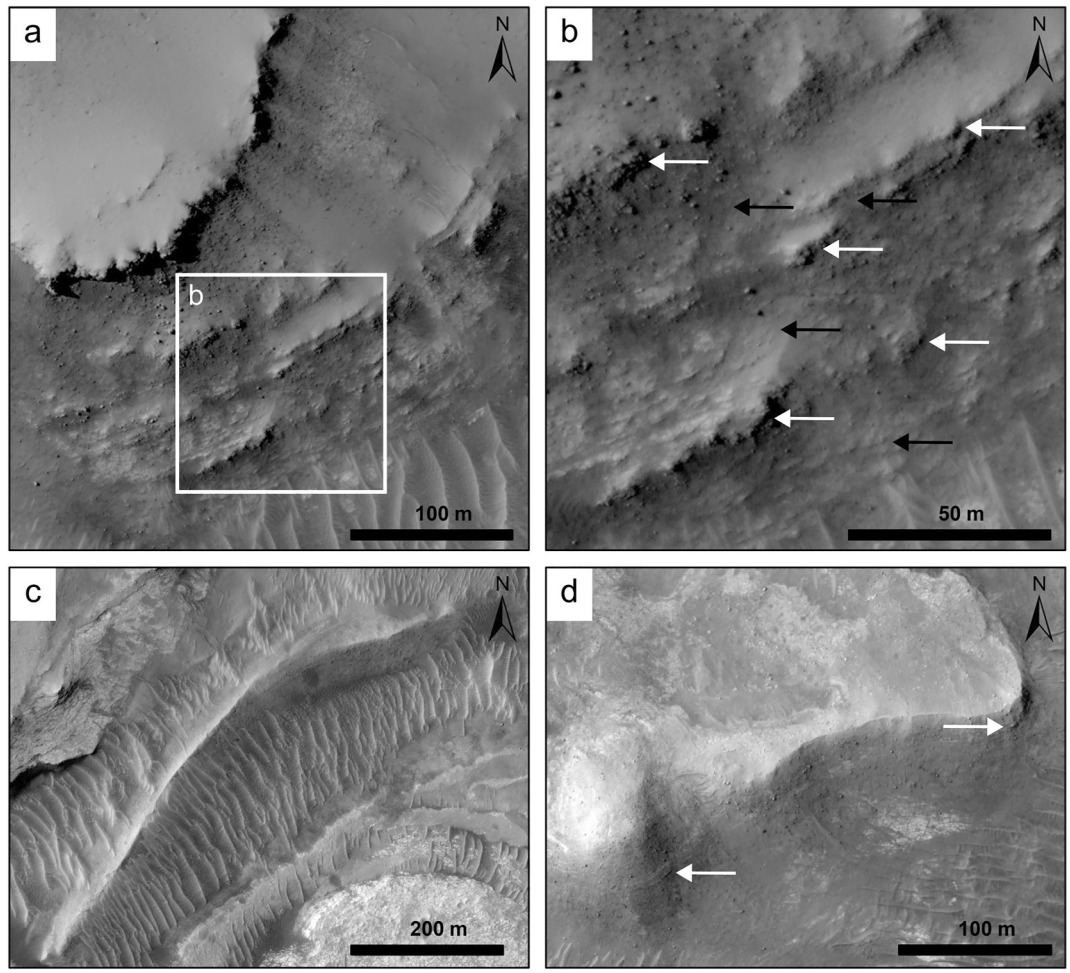

Figure 4. HiRISE image (ESP_079701_1990_RED) of layered deposits on the valley floor and walls. (a) Stratified sedimentary deposits ~50 m high composed of alternating fine-grained deposits and boulder-rich strata. (b) Close up of the alternating strata in Figure 4a. Black arrows indicate fine-grained strata and white arrows align meter-scale boulders. (c) Elongated fine-grained deposit on the valley floor with some isolated boulders. (d) Fine-grained sedimentary deposit with some boulder-bearing strata (white arrows).

The lack of inner channels is not a proof of their past absence due to preservation issues (i.e., late erosion, infilling by dunes, or landslides) and overall a low number reported on Mars (Irwin, Craddock, & Howard, 2005). Nevertheless, such an absence suggests that either the fluvial activity did not carve a channel within the existing valley or that such a channel only be locally visible, as is the case in several other valleys on Mars (e.g., Bouley et al., 2010; Irwin, Craddock, & Howard, 2005). A possible explanation for this absence is that the valley was carved by a channel occupying the entire width of the valley, at least for the last episode that removed several previous deposits.

3.3. Topographic Cross-Sections of Pliva Vallis

3.3.1. Cross-Section Along the Valley

Valley width and depth both decrease downstream (Figure 5). In Figure 5, topographic profile A is furthest upstream. At this point, the valley is 2.1 km wide and around 280 m deep, while the valley becomes 1.4 km wide and 120 m deep at the profile B, 8.5 km downstream. Continuing to the topographic profile C, the width and depth of the valley continue to decrease but more slowly, tending to stabilize at profile D. At its terminus, the valley fades into the surrounding plains and we can no longer provide any constraints on valley topography. This pattern

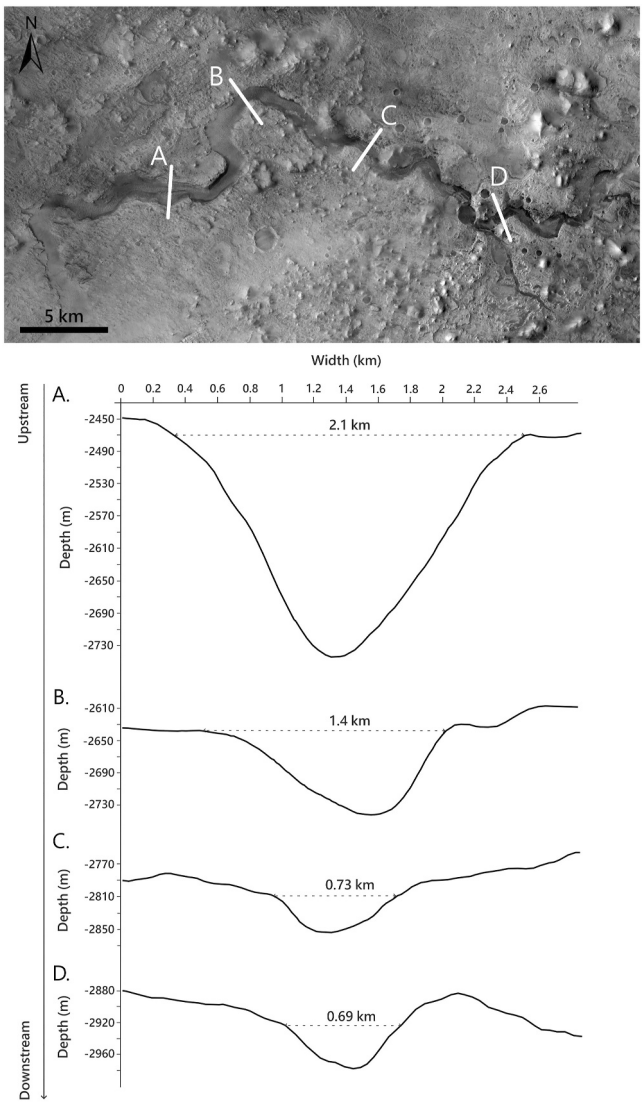

Figure 5. (top) General morphology of the outlet valley in CTX mosaic (MurrayLab_CTX_V01_E76_N16_Mosaic) with the position of the four profiles below marked by white lines. (bottom) The four topographic profiles A-D, which are derived from CTX DTMs (UDL_CTX-Mosaic_DEM_Jezero-tile-0 and UDL_CTX-Mosaic_DEM_Jezero-tile-1), illustrate the decrease in depth and width of Pliva Vallis from upstream to downstream.

is not typical of fluvial erosion, for which valleys tend to widen downstream (Schumm & Ethridge, 1994). We return to this property in Section 5.1.

3.3.2. Local Topographic Steps Along Valley Sides

HiRISE images and DTMs show that the first bend in the valley (Figures 2 and 6a), located a few kilometers from the lake outlet breach, has an irregular cross-section with several levels located at different elevations along its southern inner side. A cross section, perpendicular to the valley (Figure 6b) and shown by the blue line in Figure 6a, shows four main topographic steps, marked by the four colored lines used in Figure 6. The red line indicates the elevation (ca. −2,465 m) of the first topographical step identified in this region. The second topographic step is at ca. −2,520 m in purple, the third at −2,553 m in green and the last at −2,568 m in yellow. The valley (and the topographic steps) are shown in 3D in Figure 6c.

3.3.3. Perched Secondary Channel

A shallow perched valley, connected to the main valley, is seen on the outer bank of a valley bend (Figures 7a and 7b). The floor of this small and short perched channel is higher in elevation than the main valley floor. This is illustrated in Figures 7c and 7d, which show the topographic profile a-b across the main valley and the floor of the perched valley. This perched valley is ∼100 m wide, around 6 km long and a few meters deep. At the breach the valley is ∼720 m wide and ∼20 m deep.

3.3.4. Interpretation

The valley narrows and shallows downstream (Figure 5). By contrast, bedrock valleys on Earth usually widen downstream. In absence of any tributary and climate variations from upstream to downstream, in the case of a steady flow, the width of the valley should, at least, remain stable along its course. This decrease in depth and width reflects a loss of flow intensity from upstream to downstream, which may reflect a lack of continuity in flow and/or a loss of water by infiltration and evaporation.

We interpret the four topographic steps identified in Figure 6 as erosional terraces made by bedrock incision created by four or more distinct river flow events (Goudge & Fassett, 2018). In this interpretation, each flow event would be produced by a new breach event on the eastern edge of the lake. The only alternative explanation of the erosional terraces would be that they are an erosional expression of the layering in the bedrock of the valley wall. However, such topographic steps are not observed in other locations nearby, suggesting that the bedrock does not erode out preferentially like this by wind activity. Thus, we propose that these steps are related to at least four lake overflow events, one event for each of the terraces shown in Figure 6. (a) The first overflow event floods the terrain to the east of the crater before incising a preferential valley. Figure 6 shows the location of this first incision between the terraces at −2,465 and −2,520 m. (b) The second breach and overflow event re-uses the valley created during the first overflow and continues the incision of the valley. This second incision is located between the terraces at −2,520 and −2,553 m. (c) The third event continues to incise the valley created and deepened by the previous two episodes. In Figure 6, this event is between the terraces at −2,553 and −2,568 m. The third event seems to be the smallest overflow event. (d) A fourth and last event is identified between the terrace at −2,568 m and the valley floor at −2,630 m. The real valley floor may be a little deeper than measured because we can observe a late eolian infilling of unknown thickness.

Using the elevations of the four terraces identified in Figure 6, we reconstruct the lake level elevations at the breach between each episode. The maximum lake level is set at −2,243 m (Salese et al., 2020). At the end of the

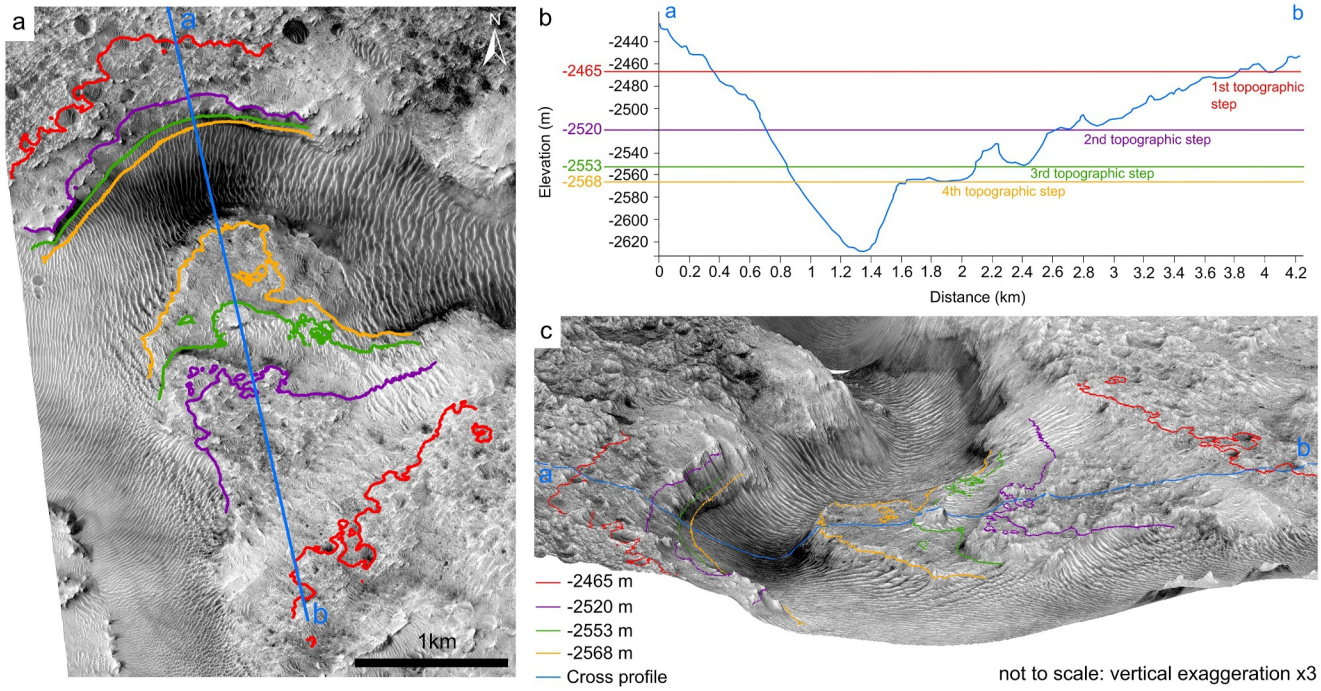

Figure 6. Identification and location of four topographic steps at the first bend in the valley. (a) HiRISE image (ESP_033717_1990_RED) of the region where we identified the main four topographic steps as indicated by the four colored contour lines. The blue line shows the location of the cross-profile where these four steps can be identified. (b) Cross-profile using topographic data from HiRISE DTM (DTEED_033651_1990_033717_1990_A01) in blue and identification of the four main topographic steps, indicated by the four colored lines. (c) 3D representation of this region where the topographic steps are shown as four colored lines. The view is looking from the west toward the east.

first episode, the lake reaches an altitude of −2,297 m, and then at the end of the second episode, the water level drops to −2,333 m. At the end of the third episode, the water level reaches −2,347 m, ending up at −2,390 m at the end of the last episode.

Lastly, we interpret the presence of the perched valley (Figure 7) as an alternative flow path used by the flood during the first episode. Indeed, the fact that the valley is perched, that is, higher in altitude than the present-day valley floor, means that this valley was not incised by the last episode. Hence, the water incised this valley during one of the first overflow events, such as for distributary channels, but the distributary was subsequently abandoned. This observation is consistent with the hypothesis of discontinuous episodic flows.

Several of these observations run counter to a valley geometry formed by steady-state flows, which are the usual form of outlet flows in an open lake system. The morphology of Pliva Vallis is more compatible with several brief flows caused by several phases of breach on the eastern edge of the Jezero Crater. From the erosional terraces, we estimated the minimum number of incisions to be four.

3.4. Longitudinal Profile of Pliva Vallis

3.4.1. Description of the Valley Floor Slope

The along-valley topographic profiles (Figure 8) once again highlight the atypical characteristics of this valley. The longitudinal profile of the valley floor (Figure 8, black profile) shows the outlet breach of the lake at an altitude of −2,390 m. Once beyond the outer rim of the crater, the gradient is negative, around −0.028 from kilometer 15 to kilometer 26. From the 26th kilometer to the end of the valley, the gradient shallows to around −0.009. Where the gradient is gentler, we observe several humps in valley-floor topography. (a) The first topographic hump is located at arrow A on the black profile in Figure 8 and (rising 83 m over 5 km), (b) the second topographic hump is at B (rising 27 m over a distance <2 km), (c) the third hump (location C) corresponds to a topographic rise of 49 m over a distance of 2.5 km.

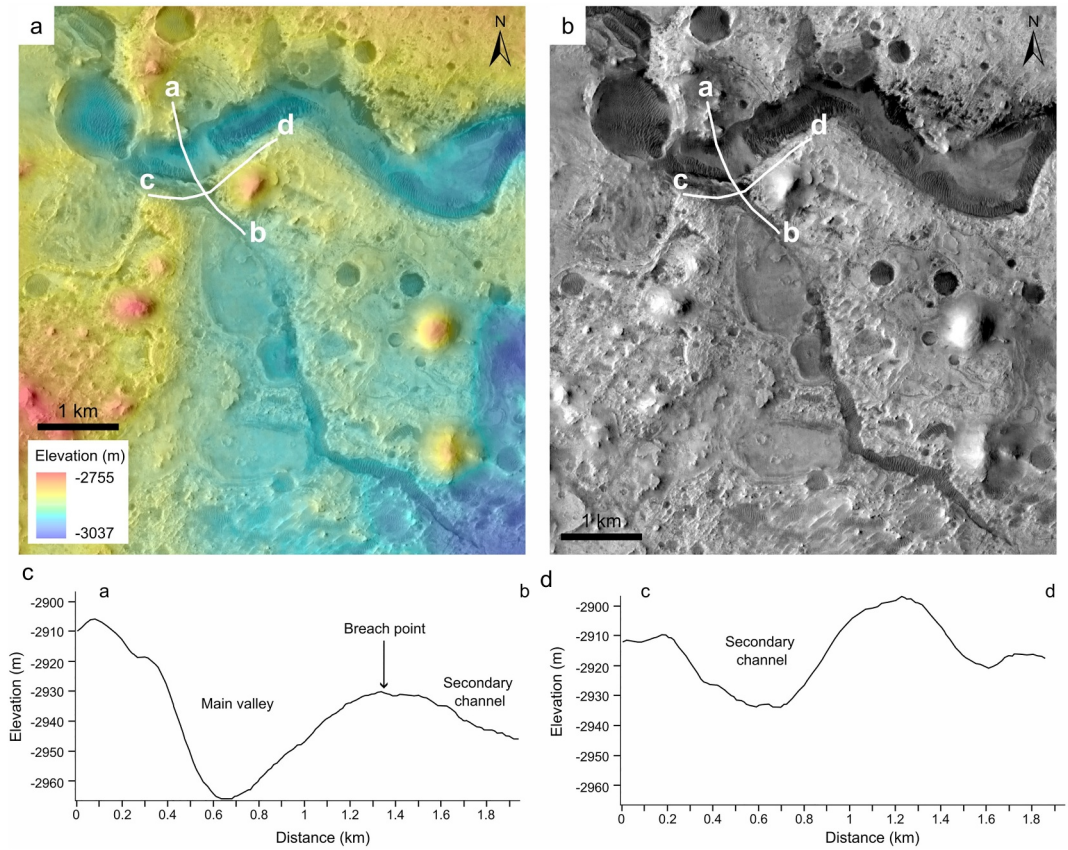

Figure 7. (a) Semitransparent CTX mosaic (CTX_V01_E76_N16_Mosaic) overlain on the colorized DTM (UDL_CTX-Mosaic_DEM_Jezero-tile-1) of the perched channel fork. (b) CTX mosaic view of the perched channel fork. The profiles in c and d are marked as white lines. (c) Cross-profile of the main valley including the breach point and the floor of the perched secondary channel to the right. (d) Cross-profile of the secondary channel at the breach point.

To compare the outlet valley long profile with that of the surrounding plateaus, we draw topographic profiles on the valley's northern (dashed profile in Figure 8) and southern shoulders (dotted profile in Figure 8). In both cases, after the breach and the crater rim, the gradient is very gentle (around −0.0025) for 8–10 km. On the remainder of the profiles, the slope of the plateau is then −0.012. The highs on the topographic profile of the valley shoulders correspond to the hummocky surface of the olivine-rich unit. On the profile of the northern shoulder, we observe two main hills (b and c on the dashed profile) and one hill on the profile of the southern shoulder (a on the dotted profile).

The context map of the valley (Figure 8) shows that these hills coincide with the humps in the valley floor. Figure 9a shows the planform configuration of the most upstream local high, where the valley rises gently to the high point. Hill *a* (identified on the dotted profile in Figure 8) is located directly to the east of the high. The valley floor is covered by aeolian dunes.

A hill several hundred meters high is located to the NE of the second downstream local high (Figure 9b and corresponding to *b* on the dashed profile in Figure 8). On the southern edge of the valley, there is a topographic rise on the valley floor that may be the deposits of a landslide that occurred after the valley formed or a landslide scar that would have been eroded since its formation. The valley floor is also filled with dunes.

Figure 9c shows the third local high (white cross) and a corresponding hill on the northern edge of the valley, which is several hundred meters high (corresponding to *c* on the dashed profile in Figure 8). Aeolian filling is once again observed but we can also see two deposits on the valley floor, which outcrop in the middle of the dunes. These deposits are described and identified in Section 3.2.1 as bedrock outcrops (Figures 3c and 3d).

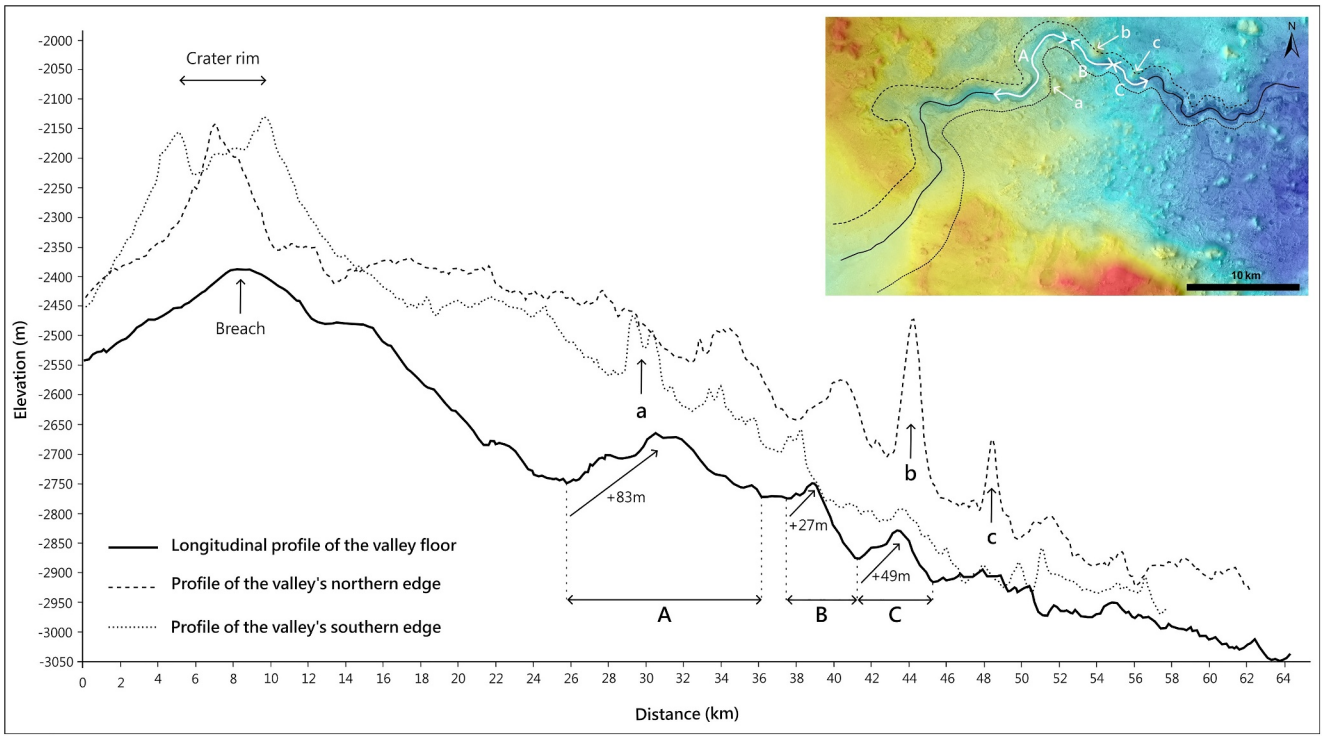

Figure 8. Longitudinal profile of the Pliva Vallis floor (black profile) and profiles of the northern and southern edges of the valley (dashed and dotted lines, respectively) using CTX DTMs (UDL_CTX-Mosaic_DEM_Jezero-tile-0 and UDL_CTX-Mosaic_DEM_Jezero-tile-1). Labels A, B and C identify the main humps on the valley floor, which are spatially correlated with topographic highs on the edges of the valley (a, b and c). The inset in the top right shows the position of the profiles on the semitransparent CTX mosaic (CTX_V01_E76_N16) overlain on the colorized DTMs (UDL_CTX-Mosaic_DEM_Jezero-tile-0 and UDL_CTX-Mosaic_DEM_Jezero-tile-1).

There are also a number of other small irregularities downstream of the valley, but they are negligible compared to those described above. One of these other irregularities is due to the presence of a crater about 1.1 km in diameter, right in the middle of the valley incision, formed after the valley incision.

3.4.2. Interpretation of the Irregularities of the Valley Floor Longitudinal Profile

Pliva Vallis drops by 600 m in 50 km, corresponding to bedrock incision. However, the three main topographic humps on the valley floor identified above are anomalous relative to expectations for river flow. One hypothesis is that these topographic humps correspond to erosionally resistant bedrock. Indeed, the three topographic highs are spatially correlated with hills on the northern and southern edges of the valley that may correspond to more resistant bedrock. The discharge must have been sufficient to overtop these barriers. The presence of fluvial sedimentary deposits and outcropping bedrock at these topographic highs and the identification of strata containing meter-sized boulders downstream in the valley supports this interpretation, as to transport such boulders the discharge must have been high. High discharge is consistent with sudden lake overflow events. However, this does not mean that the flows submerged the entirety of the topographic rises, and some of the water could have been impounded in depressions (Spence & Woo, 2003) (see Section 5.1).

Alternatively, we observe widespread modern aeolian bedforms that could have filled the valley heterogeneously to construct these humps. However, this hypothesis does not fit well with two key observations. First, we observe outcrops on the valley floor intersected by these dunes (Figure 9). In this case, the thickness of the aeolian filling cannot be as great as the topographic irregularities identified. Second, we do not observe any change in the morphology of these modern dunes that might suggest a thicker underlying deposit. Thus, we reject the hypothesis that modern dunes solely explain the humps in the valley floor topography. We also considered the hypothesis of local valley filling by impact ejecta or volcanic ash. However, there is no evidence of major impact craters or volcanoes near the valley, so we do not consider these possible modes of infill.

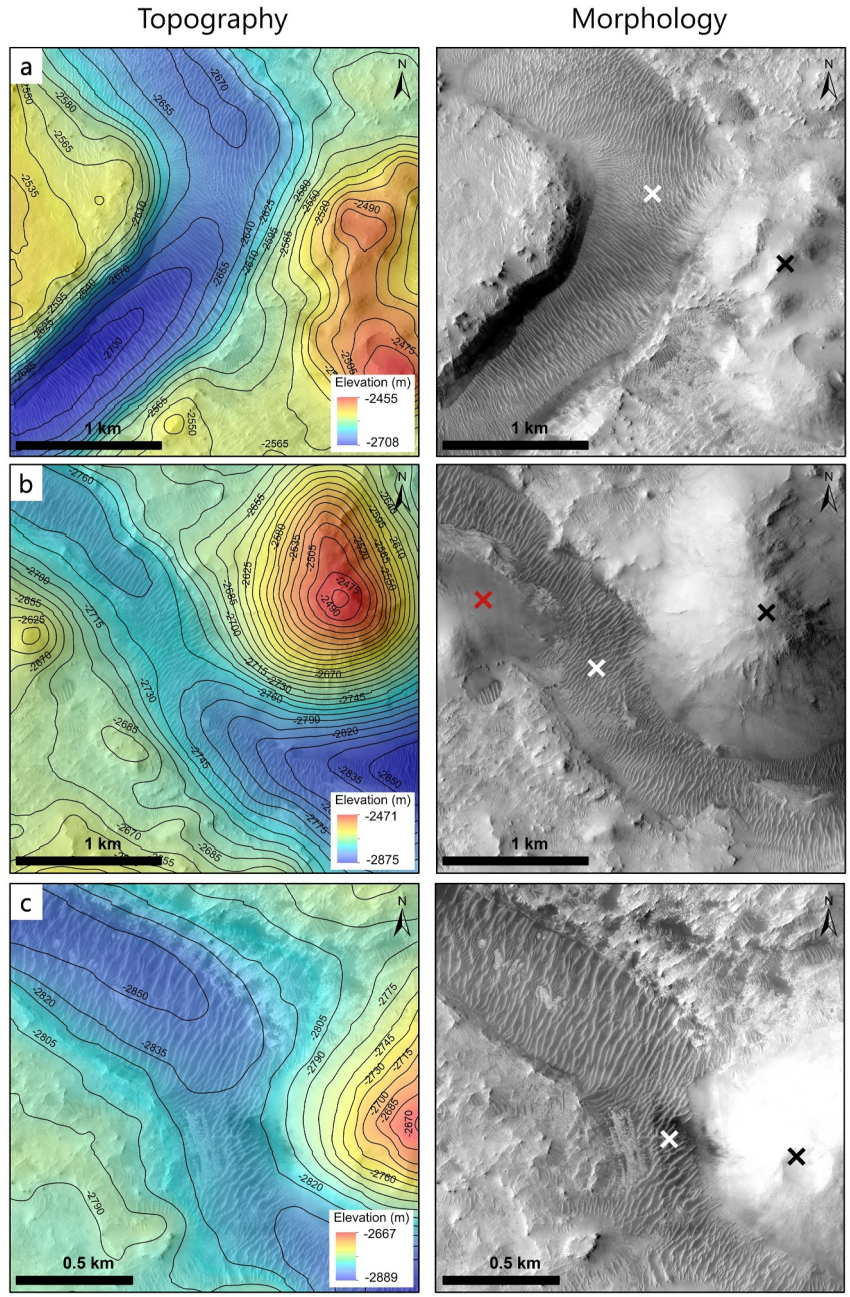

Figure 9. (left) Semitransparent HiRISE images (ESP_069310_1990_RED and ESP_069653_1990_RED) draped over colorized CTX DTMs (UDL_CTX-Mosaic_DEM_Jezero-tile-0 and UDL_CTX-Mosaic_DEM_Jezero-tile-1) with topographic contours and (right) HiRISE images to observe the morphology. The high point of each topographic rise on the valley floor is marked by a white cross (a) first hump, (b) second hump, (c) third hump, the associated hills by a black cross and possible landslide or landslide scar by a red cross.

Lastly, these humps might indicate that the valley was formed by subglacial water flow, because subglacial flows can overtop topographic rises because of the pressure of the overlying ice (e.g., Grau Galofre et al., 2018; Greenwood et al., 2007; Kehew et al., 2012). We do not favor this hypothesis based on circumstantial evidence: the lack of other valleys than Pliva Vallis in the surrounding terrains, the head of the valley at a single point on the crater rim, precisely at a topographic low, and the presence of fluvial terraces rather than subglacial deposits, but we will return to this hypothesis in Section 5.1.

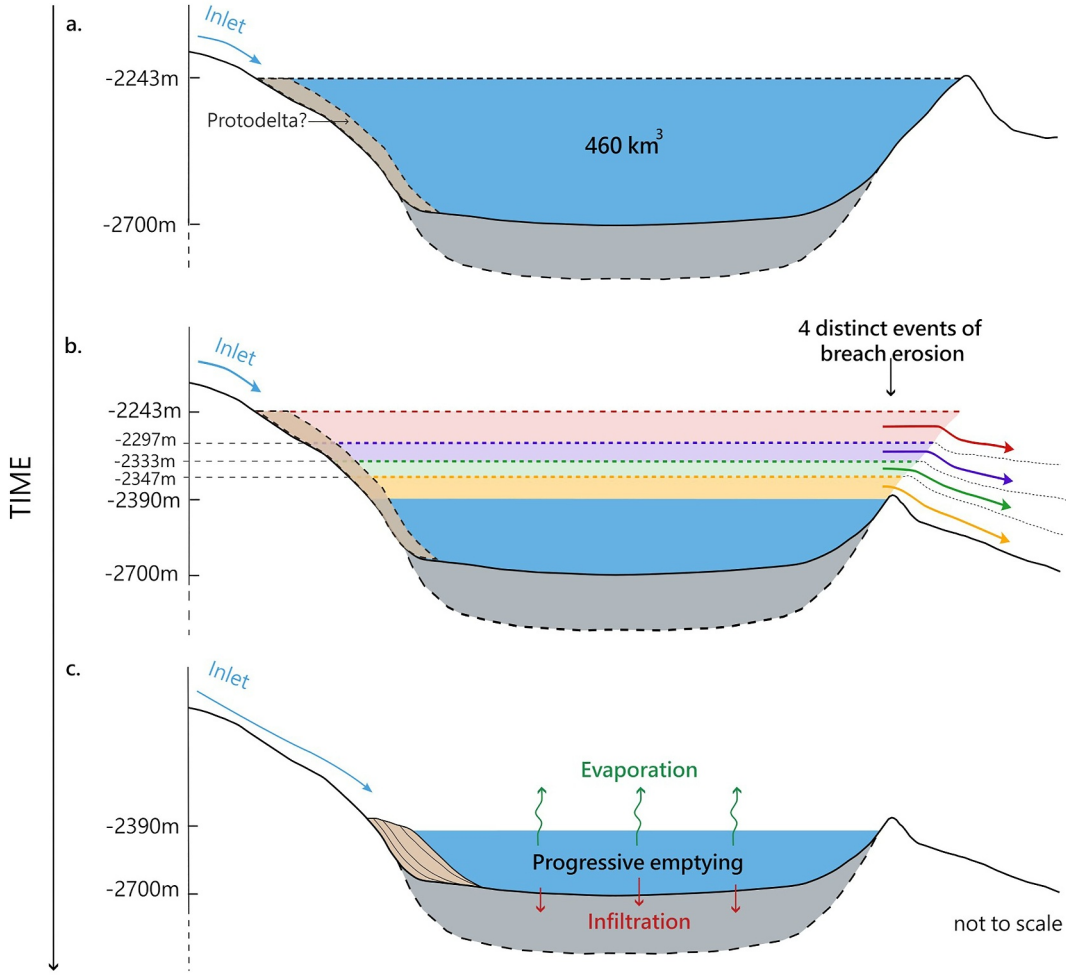

Figure 10. Scenario for the evolution of Pliva Vallis and Jezero's crater lake over time inferred from our observations. Step (a) illustrates the lake filling by one of the inlet valleys. Step (b) represents the four breach events and lake overflow. The last step (c) shows the delta formation in a closed basin during the terminal stage and progressive emptying of the lake.

3.5. Formation Scenario of Pliva Vallis

Our observations point toward a peculiar geometry of Pliva Vallis, with its shallower depth and width downstream, one perched channel (but no tributaries), an irregular longitudinal profile, and both depositional and erosional terraces. We interpret these observations as evidence for episodic rather than steady-state discharge.

Boulder-bearing sedimentary deposits in terraces indicate relatively high discharge. The presence of the valley floor humps shows that sufficient energetic flow is needed to pass these obstacles and to transport and deposit meter-sized boulders aligned in strata downstream. The topographic humps correspond to locations with hills of resistant bedrock (Figure 9). The presence of these hills on the hummocky plateau may also explain the valley's sinuous geometry described in Section 3.1. The path taken by the water flow would be constrained and guided by the topographic pattern of this hummocky terrain. Observations of incision terraces suggest four distinct events of valley incision driven by floods.

We propose the following scenario for the formation of Pliva Vallis coupled with the Jezero crater lake. First, the Jezero crater lake fills in a closed system (Figure 10a). The maximum level reached by the water is −2,243 m, an elevation constrained by Salese et al. (2020) from the topography of the inlet river Neretva Vallis.

The first breach event released a catastrophic flow onto the plateau (in red on Figure 10b). At least three other events occurred (in purple, in green and in orange in Figure 10b). At each breach event, the lake volume decreased suddenly although we do not know how much time separated each event. The irregular longitudinal profile does

not support extended steady-state flows between episodes or after the end of the fourth episode. The absence of an inner channel, although not a definitive argument as it would be in the case of the presence of a landform, and the topographic characteristics rather suggest the end of Pliva Vallis activity after the last overflow (Figure 10c).

4. Numerical Model

This section builds on the scenario inferred from the morphology to estimate the maximum flow rates for the four breach events and gives a first estimate of the duration of these four episodes based on the method proposed by Warren et al. (2021).

4.1. Discharge Estimation for the Four Overflow Events

4.1.1. Discharge Calculations

To estimate the discharge Q, we use the Darcy-Weisbach equations (Kleinhans, 2005; Wilson et al., 2004) considering the channel width W, the water height h, the local slope s_{loc}, the Martian gravity g_m (3.72 m.s^{-2}), the friction factor f and the size at which 84% of the clasts are smaller, called D_{84}. The discharge is estimated as follows:

$$Q = A \times \sqrt{\frac{8 g_m R s_{\mathrm{loc}}}{f}} \tag{1}$$

where $A = Wh$ is the cross-sectional area assuming a rectangular shape of the channel and R is the hydraulic radius, the ratio between the cross-sectional area A and the wetted perimeter $P = 2h + W$. The friction factor f is related to the roughness of the channel floor. Several experimental studies have been done to constrain the friction factor f as a function of the hydraulic radius and the grain size of the channel floor (Kleinhans, 2005; Wilson et al., 2004). Considering a gravel bed, we can express the friction factor f as follows:

$$\sqrt{\frac{8}{f}} = 5.75 \log\left(\frac{R}{D_{84}}\right) + 3.514 \tag{2}$$

By combining Equation 2 and Equation 1, we obtain the following discharge rate equation, which will be used in this paper for flow calculations in the outlet valley of Jezero crater:

$$Q = A \times \sqrt{g_m R s_{\mathrm{loc}}} \times \left(5.75 \log\left(\frac{R}{D_{84}}\right) + 3.514\right) \tag{3}$$

This equation is used because it is defined for coarse material such as boulder-bearing conglomerates, compared to sand-grain size dominated flows in which the median value (D_{50}) is used more frequently in a slightly modified version of this equation (e.g., Kleinhans, 2005).

4.1.2. Results of Discharge Calculations

To calculate the discharge $Q\left(\mathrm{m}^3.\mathrm{s}^{-1}\right)$ for each episode, we first measure in Figure 6b the width W of the valley and the water depth h which corresponds to the incision depth on the profile (e.g., the work of Larsen & Lamb, 2016). Then, we should determine the local slope s_{loc} for each event:

- For the first episode, the average slope is estimated from the local slopes of the highlands on either side of the valley. In this case, the minimum and the maximum slopes estimated for the first episode are, respectively, 0.001 and 0.01.
- For the fourth episode, we used the local slope of the valley floor. The minimum and maximum slopes estimated are, respectively, 0.028 and 0.031.
- For the second and the third episodes, the slopes are poorly constrained. For these two intermediate episodes, we tested all slopes between the minimum slope of the first episode (i.e., 0.001) and the maximum slope of the fourth episode (i.e., 0.031).

Table 1
Discharges Calculated for the Minimum and Maximum Slope Estimated for Each Overflow Event Identified

	Valley width W (m)	Depth h (m)	Local slope s_{loc} (m/m)	Discharge Q ($m^3.s^{-1}$) (Equation 3)
Episode 1	3,548	55	0.001	1.58×10^6
			0.01	4.99×10^6
Episode 2	1,923	33	0.001	3.69×10^5
			0.031	2.05×10^6
Episode 3	1,238	15	0.001	6.47×10^4
			0.031	3.6×10^5
Episode 4	720	62	0.028	1.9×10^6
			0.031	2×10^6

Other parameters to be considered in the equations are Martian gravity $g_m = 3.72$ m.s^{-2} and grain size. Here, we use a D_{84} at 0.152 m (Mangold et al., 2024), which has been found on the front of the western fan of Jezero by the SuperCam images of Perseverance rover. Although these flows are not the same flood events, the fact that they both contain boulders up to 2 m in size, similar in size to those observed by the Perseverance rover, enables a reasonable point of comparison for this value based on in situ observations. We calculated the discharge $Q\ (m^3.s^{-1})$ for each episode and for each estimated slope as described above and the results for minimum and maximum slopes are shown in Table 1, alongside the measured valley width and depth.

Figure 11 shows the calculated discharge as a function of slope for each episode. Calculated discharges are between 6.5×10^4 and 5×10^6 $m^3.s^{-1}$. These high calculated discharges, are similar to the discharge of the largest terrestrial rivers. The first episode (red line) is the most energetic episode, although with a large variability depending on slope.

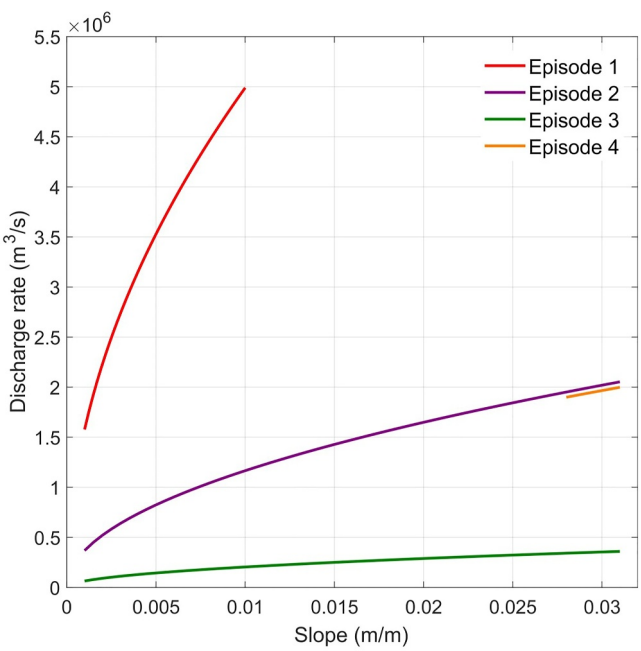

Figure 11. Discharge calculations as a function of slope for the four identified episodes.

4.2. Application of the Breach Erosion Model to the Jezero Crater Lake

4.2.1. Modeling the Overflows: The Code

The aim of the model used here is to investigate breach erosion processes and crater lake spill over with progressive emptying of the lake water rather than only estimating the highest ranges of discharges, as done in the previous section. The model used is a fixed channel width 0-D model proposed by Warren et al. (2021) and adapted from Holo and Kite (2019).

The model assumes: (a) no pre-existing valley, (b) no downstream change in the geometry of the valley (width and depth) during an episode, (c) no downstream change in flow velocity, (d) all sediments eroded are transported downstream and removed from the system, (e) the flow depth at the breach is much less than the width of the valley, (f) uniform grain size, and (g) channel width equal to valley width. Most of these assumptions are plausible according to our observations, especially the assumption that the channel width and the valley width are equal. We know that some of the sediments have been stored in the valley in places but their volume is small relative to the whole volume eroded.

We model the formation of a lake overspill bedrock valley, including flow resistance, lake draining, and sediment transport (Holo & Kite, 2019). We solve for the transport stage and the erosion rate over time.

The transport stage is a measure of the capability to transport particles in a given flow. It is expressed by the following ratio:

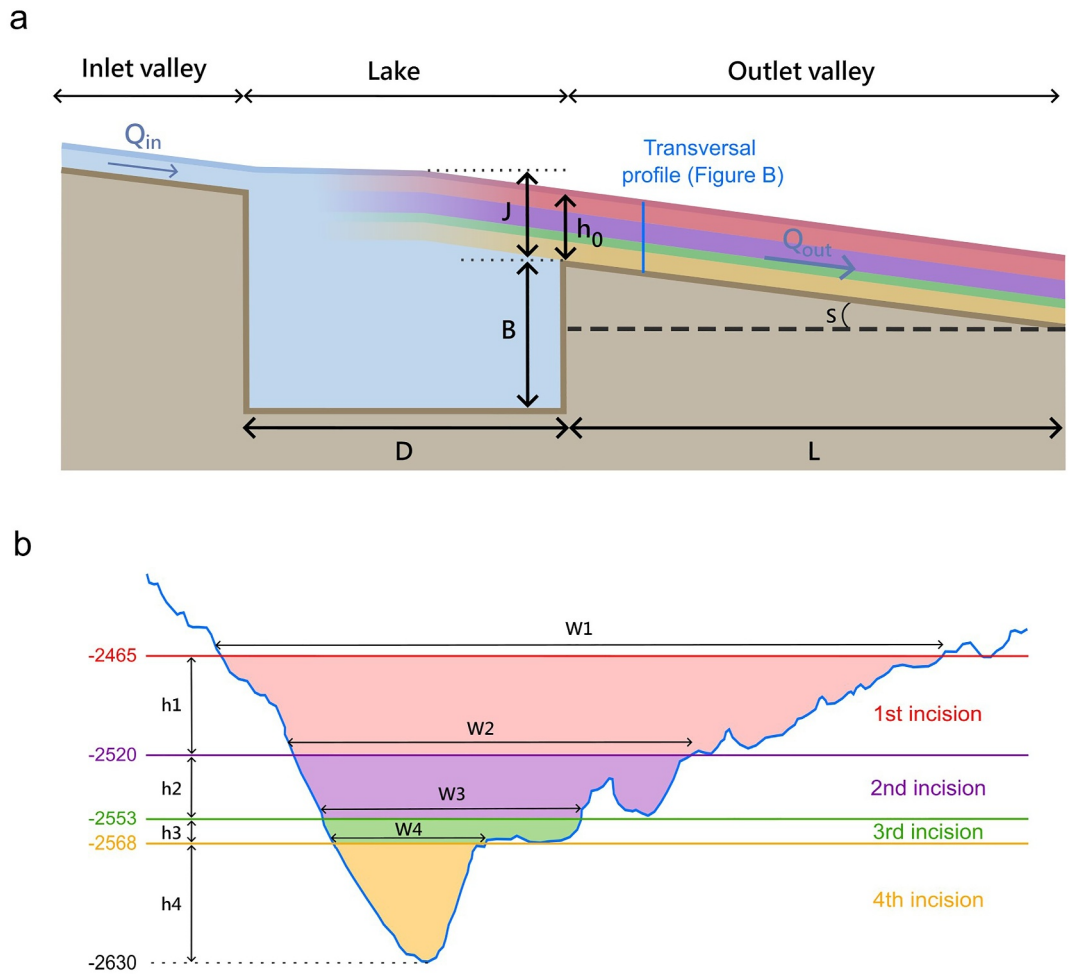

Figure 12. (a) Modeling scheme for the four breach erosion processes (adapted from Warren et al., 2021). Colors represent the different episodes identified in Figure 6. (b) Topographic cross-section used for modeling of the four breach episodes of breach and valley incision. The parameters W and h indicate the valley width and depth, respectively.

$$T = \frac{\tau_*}{\tau_{*c}} \tag{4}$$

with τ_* the Shield stress and τ_{*c} the critical Shield stress. The dimensionless shield stress is given by the following ratio:

$$\tau_* = \frac{h_0 s}{Rd} \tag{5}$$

where R is submerged specific gravity, s the channel slope at the breach, h_0 the initial flow depth and d the grain size. The variation of erosion over time is expressed by the following equation:

$$\frac{dB}{dt} = -\left(\frac{w_c}{w_v}\right) \times \frac{q_s}{L} \tag{6}$$

where B is the breach floor elevation, w_c the channel width, w_v the valley width, q_s the sediment transport and L the channel length (Figure 12a). The model assumes a rectangular shape of the valley, so $w_c = w_v = W$. To estimate the sediment transport, we use the Meyer-Peter Müller relation (Meyer-Peter & Müller, 1948) expressed by the following equation:

Table 2
Main Input Parameters for the Jezero Crater Case

Crater diameter D (km)	Valley length L (km)	Representative grain size D_{50} (m)[a]	Mars gravity g (m/s^2)	Critical shield stress τ_c [b]	Flow into crater Q_{in} ($m^3.s^{-1}$)[c,d]	Submerged gravity R[b]
45	50	0.078	3.72	0.045	100	1.8

Note. These parameters are the same for all four simulated overflow events. [a]Mangold et al. (2024). [b]Warren et al. (2021). [c]Fassett and Head (2005). [d]Salese et al. (2020).

$$q_s = 8\sqrt{Rgd^3}(\tau_* - \tau_{*c}) \quad (7)$$

with g the martian gravity.

The equations we use in the model are "transport-limited" equations. Studies by Lamb and Fonstad (2010) and Larsen and Lamb (2016) have shown that this is an appropriate assumption to describe flood events.

4.2.2. Modeling the Overflows: Input Parameters

The code was initially applied to simulate a single breach event (Warren et al., 2021). However, in Jezero crater, we infer that four breach erosion events occurred (Section 3). We chose to apply the code four times to model each event (Figures 12a and 12b). The input parameters used are described in the following section and in Table 2.

Valley geometry: The code considers the initial flow depth and the geometry of the valley measured at the breach. However, we identified the four episodes of lake overflow and valley incision few kilometers downstream of the breach (Section 3.3.2, Figure 6). Previous studies conducted by Salese et al. (2020) assumed three phases of breach and overflow, identified on the cross-section made at the breach. However, these steps are not clearly visible in the landscape when looking at 2D and 3D HiRISE images largely due to post-erosion filling by dunes. So, to apply the code at the breach, we compared the total incised area at the breach and the total incised area in the region where the four terraces are identified a few kilometers downstream. The incision at the breach is 147 m deep with a maximum valley width of 4.9 km and the total incision of the valley where terraces are identified is 165 m high with a maximum valley width of 3.5 km. The total area of the breach in the crater rim ($A_{\text{breach}} = 0.257\ \text{km}^2$) is similar to the total area of the topographic profile where we identified the four terraces ($A_{\text{profile}} = 0.247\ \text{km}^2$). Thus, we consider the region where terraces are identified to be representative of the breach geometry for the purposes of the modeling. The width and the depth of the valley for each episode are given in Table 1 (Section 4.1.2).

The grain size: We use $D_{50} = 0.078$ m (Mangold et al., 2024) for the same reason as explained in Section 4.1.2.

The initial flow depth: The initial flow depth is the flow depth at the breach just after breach failure. We test several values of initial flow depth between and 10 m and the valley depth measured for each episode.

Inlet discharge flow rate: We assume a steady-state inflow of 100 $m^3.s^{-1}$ into the lake from the inlet rivers Neretva Vallis and Sava Vallis, which is within the range estimated by previous work (50 to 200 $m^3.s^{-1}$; e.g., Fassett & Head, 2005; Salese et al., 2020) or 100 to 500 $m^3.s^{-1}$ (Mangold et al., 2024). This uncertainty is acceptable given the order of magnitude differences in discharges between this steady-state process and the overflows.

The slope: We tested a range of measured slopes for the identified episodes. The slope of the first episode corresponds to the slope of the outer crater rim (here fixed at 0.075) and for the last episode, the slope used is the slope of the valley floor measured at the breach (fixed at 0.022). For the second and third episodes, we tested a range of slopes between the slope of the fourth episode (0.022) and the slope of the first episode (0.075).

4.2.3. Modeling the Overflows: Results

Figure 13 shows the modeling results for the four breach and valley incision events. For each episode, from left to right, we give the variation of the transport stage over time, the variation of the erosion rate and the cumulative

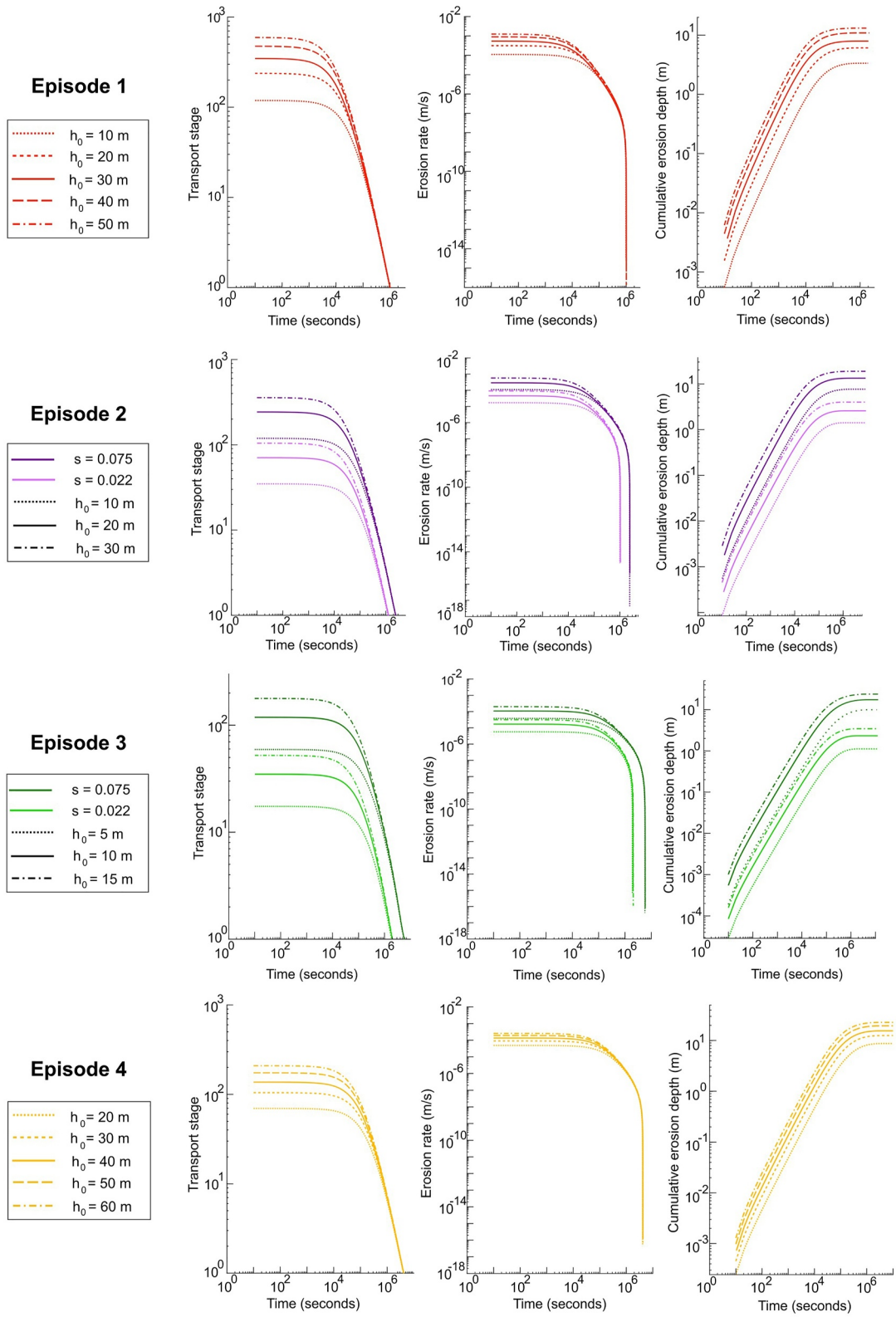

Figure 13. Modeling results for the four episodes identified in Section 3. For each episode, several initial flow depths are tested as well as several slope values for episodes 2 and 3. From left to right, we plot the transport stage as a function of time, the erosion rate as a function of time, and the cumulative eroded depth as a function of time.

Table 3
Modeling Results for Each Episode, Slope and Initial Flow Depth Tested

	Slope	Initial flow depth (m)	Final erosion depth (m)	Timescale (seconds)	Timescale (days)
Episode 1	0.075	10	3.4	9.9×10^5	11.5
		50	13.2	1.15×10^6	13.3
Episode 2	0.075	10	5.5	2.3×10^6	26.6
		30	18	2.4×10^6	27.8
	0.022	10	1.5	1.22×10^6	14.1
		30	4	1.29×10^6	14.9
Episode 3	0.075	5	10	5.7×10^6	65.9
		15	27	5.9×10^6	68.3
	0.022	5	1.2	1.9×10^6	22
		15	3.5	2.05×10^6	23.7
Episode 4	0.022	20	8.8	4.1×10^6	47.5
		60	23	4.2×10^6	48.6

eroded depth. In the model, for each episode and for all the initial flow depths tested, the transport stage decreases slowly and then rapidly over time for each episode. This decrease is due to the progressive discharge fall after breaching. When the transport stage reaches a value of 1, the flow is too weak to continue to carry particles, so erosion stops. The erosion rate follows the same trend over time: it decreases slowly at first and then rapidly when the discharge is no longer sufficient to maintain the erosion of the valley. The initial flow depth does not have a significant effect on the duration of sediment transport and erosion. However, it influences the efficiency of sediment transport and therefore of erosion, particularly at the beginning of the lake overflow. Higher initial flow depth means greater transport stage and erosion rate. Consequently, cumulative erosion over time is greater when initial flow depths are higher. Table 3 summarizes the results for each episode in terms of final erosion depth (m) and timescale (seconds and days).

In terms of timescale, the modeling results suggest that the transport of particles and erosion lasts for a few days to a few weeks per event (Figure 13 and Table 3). For the second and third episodes, the slope affects the duration of sediment transport and erosion in the valley. However, the time scale remains very rapid.

For each episode, the final erosion of the valley ranges from a few meters to around 20 m. The erosion predicted by the model is lower than the erosion measured in the outlet valley in the region where the four episodes were identified (Figure 6). These results will be discussed in Section 5.2.

5. Discussion

5.1. Sporadic Activity of Pliva Vallis

Our observations lead us to interpret Pliva Vallis as a fluvial valley formed by at least 4 distinct episodes of overflows of the Jezero lake. To accommodate the data, we propose "fill-and-spill" evolution. This process, shown in Figure 14 describes an accumulation of water in a topographic depression (Spence & Woo, 2003; Warner et al., 2013). Initially, discharge is sufficient to pour over topographic rises on the valley floor (Figure 14a). As discharge wanes (Figure 14b), water pools in the topographic depression, forming a small temporary lake within the valley. The flow feeding the outlet valley ceases and this small lake is full of water; this new lake overflows and water would spill downstream again. This progressive spill of accumulated water progressively erodes the top of the rises present in the valley floor (Figures 14c and 14d). The sediment is swept downstream.

Other possibilities for interpreting Pliva Valis formation include: (a) a valley carved by steady flows with an open lake system, (b) a valley formed by one flood, and (c) a subglacial valley. We discuss each of these alternate possibilities in turn.

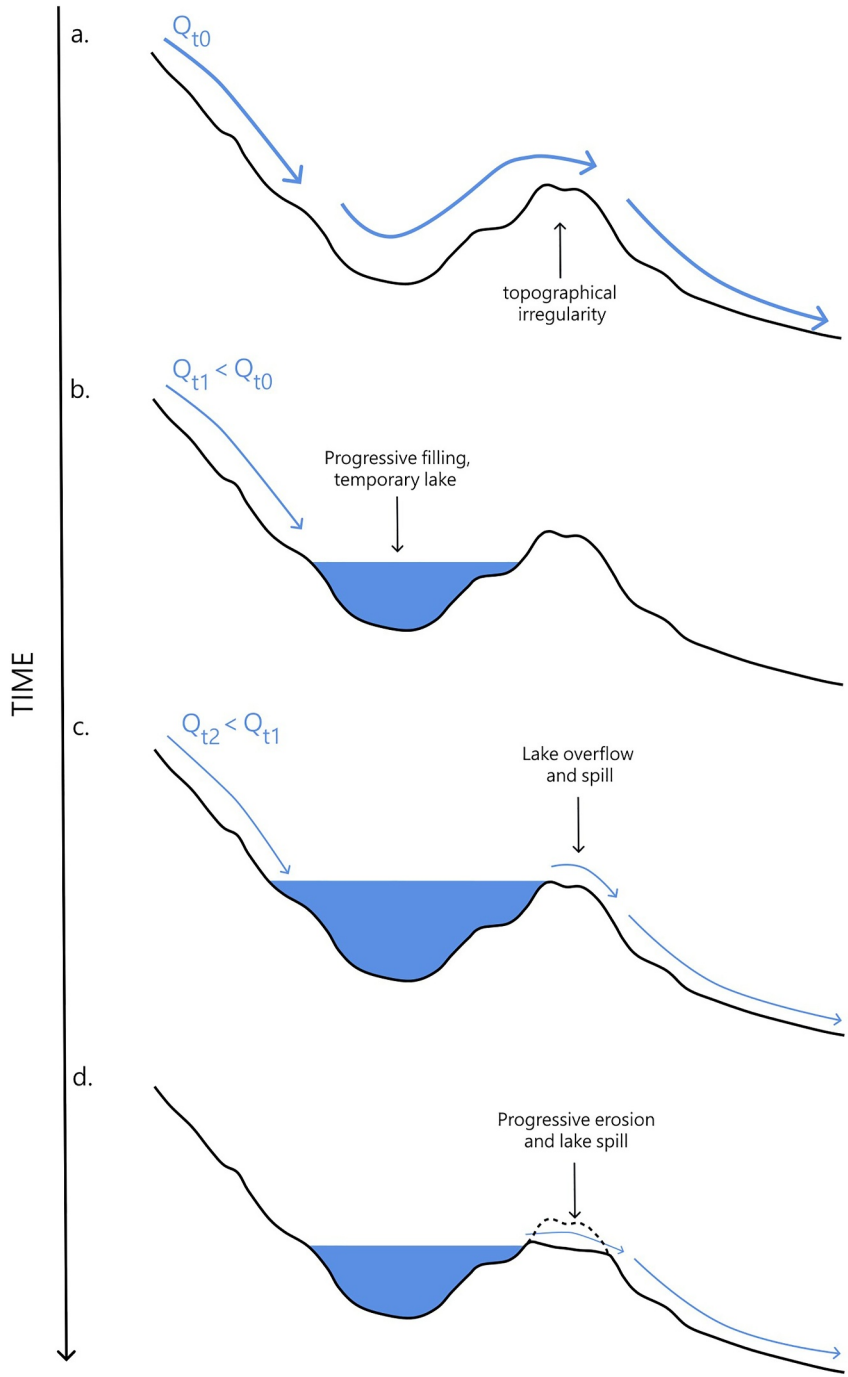

Figure 14. Sketch of the fill and spill process. (a) The flow is sufficiently energetic to overcome topographic rises after breach rupture. (b) The flow is less energetic than the initial flow. There is a progressive filling at the bottom of the topographic rise. (c) Water reaches the top of the topographic rise and flows gently again. (d) The flow of water gradually erodes the high point of the topographic highs on the valley floor.

A continuous flow cannot explain the formation of a valley like Pliva Vallis. The valley's overall morphology, marked by decreasing in depth and width from upstream to downstream, is not in line with the typical valley geometry as we know it from Earth. Normally, valley width increases downstream while depth decreases as the slope becomes gentler (Schumm & Ethridge, 1994); although there might be exception along regions with enhanced evaporation, the difference between upstream (~255 m depth) and downstream (~50 m depth) here is

huge and observed over less than 50 km. The topographic rises in the valley floor highlighted in Section 3.4 also contradict a continuous flow. A simple continuous flow would not be able to pass these rises with sufficient energy to carry boulders downstream of at least 1 m in diameter (Figure 4). However, in the fill and spill geometry proposed in Figure 14, we cannot exclude that a steady flow occurred between the phase of overflows. However, after all overflows occurred, a steady flow would have to be less intense, with discharges similar or lower to that of Neretva Vallis (estimate in the range of several 100 s of $m^3.s^{-1}$; Fassett & Head, 2005; Mangold et al., 2024 in various locations of the western fan). We do not observe deposits from such steady-flow periods nor do we observe inner channels that would have incised the topography within the valley floor. The last overflow seems to have produced a final "reset" of the valley without noticeable subsequent activity.

Rather than the four episodes of overflow that we propose, a single overflow valley has also been proposed (Holo & Kite, 2019) or (alternatively) an overflow in three phases (Salese et al., 2020). The presence of re-incised sedimentary deposits, perched valley and incision terraces in the bedrock, point to several episodes of breach erosion and hence valley incision by multiple lake overflows, thus rejecting the single-episode hypothesis for this valley incision. We also found better evidence of these episodes in the valley than at the breach where only three of them have been identified by Salese et al. (2020).

Lastly, we consider the possibility of a subglacial valley. Subglacial flows are known to overcome local topographic rises on Earth (Glasser & Smith, 1999; Grau Galofre et al., 2018; Greenwood et al., 2007; Kehew et al., 2012; Sissons, 1961). However, we have suggested in Section 3.4 that these topographic rises are due to the greater strength of the bedrock at these points, as shown by the existence of nearby hills on the valley shoulders. In addition, the general morphology of the valley shows a decrease in depth and width downstream, while subglacial channels tend to remain of similar width or become larger, as the flow regime does not decrease downstream (Carr & Malin, 2000; Grau Galofre et al., 2018). Subglacial valleys are generally wide and connected with an anastomosed pattern (Grau Galofre et al., 2018; Walder & Hallet, 1979), while there is no such a geometry in the case of Pliva Vallis, and no other such valley to the East of Jezero. Last, but not the least, the altitude of the breach is consistent with the altitude of the delta apex on the western side of Jezero, which presumably formed after the formation of the breach.

Thus, our results are more consistent with the sporadic activity of Pliva Vallis by, at least, four episodes of overflows than the alternate hypotheses. This localized result has implications for the understanding of past martian rivers in general because many include lake breaches (Goudge et al., 2021). In turn, our study shows that this process can consist of several episodes of overflows rather than just a single breach overflow event.

5.2. Model Limitations

The model has limitations and can be discussed in the same way as we have discussed other possible interpretations of the valley. The 0-D model proposed by Warren et al. (2021) gives a minimum estimate of the duration of each breach event. For each episode, the final erosion depth of the valley predicted by the model is lower than that predicted by observations and measurements. Possible explanations include the following.

First, simplifications in valley geometry in the model may lead to an underestimate of the erosion depth. For example, the geometry of the valley is approximated as a uniform valley from upstream to downstream. We saw in Section 3.3.1 that the width and depth of the valley decrease from upstream to downstream. Moreover, the water may have overflowed the valley sides at some point, as suggested by the presence of a perched secondary channel reported in Section 3.3.3. In this case, we can probably assume that the duration of these incision events may vary from what we have calculated, but they should have the same order of magnitude.

Second, the assumption of a uniform grain size is not representative of what can be observed in the orbital images. Hence, we used different grain sizes in the code to test the sensitivity of our model results to the effect of the grain size. To do this, as explained in Section 4.1.2, we used the grain size distribution of Mangold et al. (2024). Their results suggest that the most frequent grain sizes observed are between 0.038 and 0.431 m with a D_{50} of 0.078 m. We ran the code for each episode, fixing the slope and the initial flow depth and varying the modal grain size. The fixed slope used for each episode is, respectively, 0.075, 0.05, 0.04 and 0.022. Figure S2 in Supporting Information S1 illustrates the influence of the grain size on the transport capacity over time for the four episodes. We found that large grains are transported for less time than small grains for a flow of the same energy. However, in terms of the final erosion depth, the grain size does not have a significant impact on timescales. In terms of transport stage, the

largest grains are more difficult to transport than the smaller grains. Smaller grains are transported longer than the largest grains, but the time scale remains relatively short in both cases for each episode.

Third, another possible limitation concerns the number of overflow episodes identified in our study. We identified 4 major terraces in the landscape and the topography (Figure 6), and consequently 4 main episodes of breach and valley incision. However, the valley could be formed by more than four overflow events because large events can erase evidence of smaller preceding events. Such small events could incise the valley by a few meters or tens of meters, as predicted by the model. Because we have no way of knowing how many smaller events there could have been, we focus only on modeling the four events with good morphological evidence. Thus, we can conclude that Pliva Vallis is a valley formed by at least four episodes of lake overflow, each lasting at least a few days to a few weeks.

Another limitation is that the intermittency of the inlet discharge is not considered in our simulation, nor the possible role of the second inlet river, Sava Vallis, on the inlet discharge. However, a range of inlet discharges (50 to 500 $m^3.s^{-1}$, Fassett & Head, 2005; Mangold et al., 2024; Salese et al., 2020) were tested and the variation of this value has little effect on our results.

5.3. Implications for Jezero Crater Lake

Previous work interprets the Jezero paleolake as an ancient open basin (Ehlmann et al., 2008; Fassett & Head, 2005; Goudge, Mustard, et al., 2015; Schon et al., 2012). Our results show the predominance of overflows rather than a steady flow for the outlet river Pliva Vallis. Hence, our results suggest that the Jezero crater lake was mainly a closed basin episodically opened during sporadic overflows, but that may never have experienced a long period of open lake conditions.

These results are consistent with Perseverance rover observations on the delta front and Kodiak butte (Caravaca et al., 2024; Mangold et al., 2021, 2024). The observations of deltaic topsets and foresets at elevations well below that of the elevation of the breach point on the eastern crater rim are markers of a lake level well below that of the breach. The delta prograded toward the interior of the lake, decreasing in altitude as it advanced into a shrinking lake. The apex of the delta is at the same elevation as the breach, but delta topset deposits are found at lower elevations. Thus, it is likely that the delta was formed after the overflow events and during the lake regression rather than during the filling of the lake (Figure 10c). These results have implications for the understanding of the Jezero lake system, for example, its evolution over time, which would be controlled by precipitation-evaporation balance in the absence of outflow (e.g., Horvath & Andrews-Hanna, 2024). In particular, these results imply an influence on the geochemistry of the lake, that is, an increase in salinity potentially leading to the formation of evaporites, given that the sedimentary deposition in a closed lake differs from that in an open lake system (Fukushi et al., 2019).

6. Conclusion

We report that Pliva Vallis, the 50 km long outlet valley of the Jezero crater lake, has several fluvial layered sedimentary deposits on its floor and walls. HiRISE images show alternating fine-grained deposits and meter-scale boulders, suggesting variability in the intensity of the flow creating the deposits. The valley has the following atypical characteristics: (a) a decrease in the valley width and depth from upstream to downstream, which is not consistent with a steady flow over time, and (b) the presence of a perched valley as well as topographic rises on the valley floor, which together suggest a discontinuous and energetic fluvial regime of the outlet valley. In addition, re-incised fluvial deposits and, at least, four bedrock incision terraces on the upstream part of the valley wall are consistent with a strong variability in the fluvial regime of the valley. To account for these observations, we propose a scenario with at least four main episodes of overflow and valley incision. Modeling, gives a minimum estimate of the duration of these episodes of a few days or a few weeks, consistent with our interpretation of discontinuous incision of Pliva Vallis by sporadic fluvial regimes. This study helps us better constrain the activity of the upstream lake. We propose a new scenario for the history of the Jezero crater lake, as a predominantly closed system, which was episodically and temporarily opened during at least the four identified overflow events but never experienced long-term open system conditions.

Data Availability Statement

All images and DTMs used in this study are available online. CTX images are available using the following link: https://murray-lab.caltech.edu/CTX/V01/tiles/. The four CTX DTMs used are available using the following link: https://marssi.univ-lyon1.fr/data/MARS/MRO/CTX/Jezero/. HiRISE images and DTMs used are available using the following links: https://www.uahirise.org/ESP_080545_1985, https://www.uahirise.org/ESP_021678_1985, https://www.uahirise.org/ESP_011630_1985, https://www.uahirise.org/ESP_033717_1990, https://www.uahirise.org/ESP_080927_1990, https://www.uahirise.org/ESP_069310_1990, https://www.uahirise.org/ESP_069653_1990, https://www.uahirise.org/ESP_079701_1990, https://www.uahirise.org/ESP_026359_1990, https://www.uahirise.org/ESP_026359_1990, https://www.uahirise.org/ESP_049343_1990, https://www.uahirise.org/ESP_028970_1990. The Matlab code used to produce Figures 11 and 13 is available on Zenodo at https://doi.org/10.5281/zenodo.15183051 (Villette et al., 2025).

Acknowledgments

The authors are grateful to Emily Bamber and Virginia Gulick for their helpful comments that have helped us to improve the manuscript. French authors have been financially supported by the French Space Agency—Centre National d'Etudes Spatiales (CNES) and the INSU (Institut National des Sciences de l'Univers) of CNRS (Centre National de Recherche Scientifique) in the framework of the International Research Center (IRC) between the University of Chicago and CNRS. The CTX DEM has been processed with the MarsSI (marssi.univ-lyon1.fr) application founded by the European Union's Seventh Framework Program (FP7/2007–2013) (ERC Grant Agreement 280168). We acknowledge the support from France and Chicago Cooperating in the Sciences (FACCTS) program.

References

Bouley, S., Craddock, R. A., Mangold, N., & Ansan, V. (2010). Characterization of fluvial activity in Parana Valles using different age-dating techniques. *Icarus*, *207*(2), 686–698. https://doi.org/10.1016/j.icarus.2009.12.030

Cabrol, N. A., & Grin, E. A. (1999). Distribution, classification, and ages of Martian impact crater lakes. *Icarus*, *142*(1), 160–172. https://doi.org/10.1006/icar.1999.6191

Cabrol, N. A., & Grin, E. A. (2001). The evolution of lacustrine environments on Mars: Is Mars only hydrologically dormant? *Icarus*, *149*(2), 291–328. https://doi.org/10.1006/icar.2000.6530

Cabrol, N. A., & Grin, E. A. (2010). *Lakes on Mars*. Elsevier Science. https://doi.org/10.1016/C2009-0-06633-1

Caravaca, G., Dromart, G., Mangold, N., Gupta, S., Kah, L. C., Tate, C., et al. (2024). Depositional facies and sequence stratigraphy of Kodiak butte, western delta of Jezero Crater Mars. *Journal of Geophysical Research: Planets*, *129*(3), e2021JE007023. https://doi.org/10.1029/2023JE008205

Carr, M. H. (1987). Water on Mars. *Nature*, *326*(6108), 30–35. https://doi.org/10.1038/326030a0

Carr, M. H., & Malin, M. C. (2000). Meter-cale characteristics of Martian channels and valleys. *Icarus*, *146*(2), 366–386. https://doi.org/10.1006/icar.2000.6428

Carr, M. H., Masursky, H., Baum, W. A., Blasius, K. R., Briggs, G. A., Cutts, J. A., et al. (1976). Preliminary results from the Viking orbiter imaging experiment. *Science*, *193*(4255), 766–776. https://doi.org/10.1126/science.193.4255.766

De Hon, R. A. (1992). Martian lake basins and lacustrine plains. *Earth, Moon, and Planets*, *56*(2), 95–122. https://doi.org/10.1007/BF00056352

Dickson, J. L., Ehlmann, B. L., Kerber, L. A., & Fassett, C. I. (2024). The global context camera (CTX) mosaic of Mars: A product of information-preserving image data processing. *Earth and Space Science*, *11*(7), e2024EA003555. https://doi.org/10.1029/2024EA003555

Dickson, J. L., Kerber, L. A., Fassett, C. I., & Ehlmann, B. L. (2018). A global, blended CTX mosaic of Mars with vectorized seam mapping: A new mosaicking pipeline using principles of non-destructive image editing. In *Lunar and planetary science conference (LPSC 2018)*. Retrieved from https://www.hou.usra.edu/meetings/lpsc2018/pdf/2480.pdf

Ehlmann, B. L., Mustard, J. F., Murchie, S. L., Poulet, F., Bishop, J. L., Brown, A. J., et al. (2008). Orbital identification of carbonate-bearing rocks on Mars. *Science*, *322*(5909), 1828–1832. https://doi.org/10.1126/science.1164759

Farley, K. A., Stack, K. M., Shuster, D. L., Horgan, B. H. N., Hurowitz, J. A., Tarnas, J. D., et al. (2022). Aqueously altered igneous rocks sampled on the floor of Jezero crater, Mars. *Science*, *377*(6614), eabo2196. https://doi.org/10.1126/science.abo2196

Fassett, C. I., & Head, J. W. (2005). Fluvial sedimentary deposits on Mars: Ancient deltas in a crater lake in the Nili Fossae region. *Geophysical Research Letters*, *32*(14), 1–5. https://doi.org/10.1029/2005GL023456

Fassett, C. I., & Head, J. W. (2008a). Valley network-fed, open-basin lakes on Mars: Distribution and implications for Noachian surface and subsurface hydrology. *Icarus*, *198*(1), 37–56. https://doi.org/10.1016/j.icarus.2008.06.016

Fassett, C. I., & Head, J. W. (2008b). The timing of Martian valley network activity: Constraints from Buffered Crater Counting. *Icarus*, *195*(1), 61–89. https://doi.org/10.1016/j.icarus.2007.12.009

Fukushi, K., Sekine, Y., Sakuma, H., Morida, K., & Wordsworth, R. (2019). Semiarid climate and hyposaline lake on early Mars inferred from reconstructed water chemistry at Gale. *Nature Communications*, *10*(4896), 4896. https://doi.org/10.1038/s41467-019-12871-6

Glasser, N. F., & Smith, G. H. S. (1999). Glacial meltwater erosion of the Mid-Cheshire Ridge: Implications for ice dynamics during the Late Devensian glaciation of northwest England. *Journal of Quaternary Science*, *14*(7), 703–710. https://doi.org/10.1002/(SICI)1099-1417(199912)14:7<703::AID-JQS465>3.0.CO;2-9

Goldspiel, J. M., & Squyres, S. W. (1991). Ancient aqueous sedimentation on Mars. *Icarus*, *89*(2), 392–410. https://doi.org/10.1016/0019-1035(91)90186-W

Goudge, T. A., Aureli, K. L., Head, J. W., Fassett, C. I., & Mustard, J. F. (2015). Classification and analysis of candidate impact crater-hosted closed-basin lakes on Mars. *Icarus*, *260*, 346–367. https://doi.org/10.1016/j.icarus.2015.07.026

Goudge, T. A., & Fassett, C. I. (2018). Incision of Licus Vallis, Mars, from multiple lake overflow floods. *Journal of Geophysical Research: Planets*, *123*(2), 405–420. https://doi.org/10.1002/2017JE005438

Goudge, T. A., Head, J. W., Mustard, J. F., & Fassett, C. I. (2012). An analysis of open-basin lake deposits on Mars: Evidence for the nature of associated lacustrine deposits and post-lacustrine modification processes. *Icarus*, *219*(1), 211–229. https://doi.org/10.1016/j.icarus.2012.02.027

Goudge, T. A., Morgan, A. M., Stucky de Quay, G., & Fassett, C. I. (2021). The importance of lake breach floods for valley incision on early Mars. *Nature*, *597*(7878), 645–649. https://doi.org/10.1038/s41586-021-03860-1

Goudge, T. A., Mustard, J. F., Head, J. W., Fassett, C. I., & Wiseman, S. M. (2015). Assessing the mineralogy of the watershed and fan deposits of the Jezero Crater paleolake system, Mars. *Journal of Geophysical Research: Planets*, *120*(4), 775–808. https://doi.org/10.1002/2014JE004782

Grau Galofre, A., Jellinek, A. M., Osinski, G. R., Zanetti, M., & Kukko, A. (2018). Subglacial drainage patterns of Devon Island, Canada: Detailed comparison of rivers and subglacial meltwater channels. *The Cryosphere*, *12*(4), 1461–1478. https://doi.org/10.5194/tc-12-1461-2018

Greenwood, S. L., Clark, C. D., & Hughes, A. L. C. (2007). Formalising an inversion methodology for reconstructing ice-sheet retreat patterns from meltwater channels: Application to the British ice sheet. *Journal of Quaternary Science*, *22*(6), 637–645. https://doi.org/10.1002/jqs.1083

Hoke, M. R. T., & Hynek, B. M. (2009). Roaming zones of precipitation on ancient Mars as recorded in valley networks. *Journal of Geophysical Research*, *114*(E8), E08002. https://doi.org/10.1029/2008JE003247

Holo, S. J., & Kite, E. S. (2019). Dynamics of Mars lake-overflow valley incision. In *50th lunar and planetary science conference (LPSC 2019)*. Retrieved from https://www.hou.usra.edu/meetings/lpsc2019/pdf/2481.pdf

Horgan, B. H. N., Anderson, R. B., Dromart, G., Amador, E. S., & Rice, M. S. (2020). The mineral diversity of Jezero crater: Evidence for possible lacustrine carbonates on Mars. *Icarus*, *339*, 113526. https://doi.org/10.1016/j.icarus.2019.113526

Horvath, D. G., & Andrews-Hanna, J. C. (2024). The hydrology of the Jezero crater paleolake: Implications for the climate and limnology of the lake system from hydrological modeling. *Earth and Planetary Science Letters*, *635*, 118690. https://doi.org/10.1016/j.epsl.2024.118690

Howard, A. D., Moore, J. M., & Irwin, R. P. (2005). An intense terminal epoch of widespread fluvial activity on early Mars: 1. Valley network incision and associated deposits. *Journal of Geophysical Research*, *110*(E12), E12S14. https://doi.org/10.1029/2005JE002459

Irwin, R. P., Craddock, R. A., & Howard, A. D. (2005). Interior channels in Martian valley networks: Discharge and runoff production. *Geology*, *33*(6), 489–492. https://doi.org/10.1130/G21333.1

Irwin, R. P., Howard, A. D., Craddock, R. A., & Moore, J. M. (2005). An intense terminal epoch of widespread fluvial activity on early Mars: 2. Increased runoff and paleolake development. *Journal of Geophysical Research*, *110*(E12), E12S15. https://doi.org/10.1029/2005JE002460

Kehew, A. E., Piotrowski, J. A., & Jørgensen, F. (2012). Tunnel valleys: Concepts and controversies — A review. *Earth-Science Reviews*, *113*(1–2), 33–58. https://doi.org/10.1016/j.earscirev.2012.02.002

Kirk, R. L., Mayer, D. P., Fergason, R. L., Redding, B. L., Galuszka, D. M., Hare, T. M., & Gwinner, K. (2021). Evaluating stereo digital terrain model quality at Mars rover landing sites with HRSC, CTX, and HiRISE images. *Remote Sensing*, *13*(17), 3511. https://doi.org/10.3390/rs13173511

Kite, E. S., & Noblet, A. (2022). High and dry: Billion-year trends in the aridity of river-forming climates on Mars. *Geophysical Research Letters*, *49*(24), e2022GL101150. https://doi.org/10.1029/2022GL101150

Kleinhans, M. G. (2005). Flow discharge and sediment transport models for estimating a minimum timescale of hydrological activity and channel and delta formation on Mars. *Journal of Geophysical Research*, *110*(E12), E12003. https://doi.org/10.1029/2005JE002521

Kremer, C. H., Mustard, J. F., & Bramble, M. S. (2019). A widespread olivine-rich ash deposit on Mars. *Geology*, *47*(7), 677–681. https://doi.org/10.1130/G45563.1

Lamb, M. P., & Fonstad, M. A. (2010). Rapid formation of a modern bedrock canyon by a single flood event. *Nature Geoscience*, *3*, 477–481. https://doi.org/10.1038/ngeo894

Larsen, I., & Lamb, M. (2016). Progressive incision of the Channeled Scablands by outburst floods. *Nature*, *538*(7624), 229–232. https://doi.org/10.1038/nature19817

Malin, M. C., Bell, J. F. III, Cantor, B. A., Caplinger, M. A., Calvin, W. M., Clancy, R. T., et al. (2007). Context camera investigation on board the Mars reconnaissance orbiter. *Journal of Geophysical Research*, *112*(E5), E05S04. https://doi.org/10.1029/2006JE002808

Mandon, L., Quantin-Nataf, C., Thollot, P., Mangold, N., Lozac'h, L., Dromart, G., et al. (2020). Refining the age, emplacement and alteration scenarios of the olivine-rich unit in the Nili Fossae region, Mars. *Icarus*, *336*, 113436. https://doi.org/10.1016/j.icarus.2019.113436

Mangold, N., Adeli, S., Conway, S., Ansan, V., & Langlais, B. (2012). A Chronology of Early Mars climatic evolution from impact crater degradation. *Journal of Geophysical Research*, *117*(E4), E04003. https://doi.org/10.1029/2011JE004005

Mangold, N., Caravaca, G., Gupta, S., Williams, R. M. E., Dromart, G., Gasnault, O., et al. (2024). Architecture of fluvial and deltaic deposits exposed along the eastern edge of the western fan of Jezero crater, Mars. *Journal of Geophysical Research: Planets*, *129*(3), e2023JE008204. https://doi.org/10.1029/2023JE008204

Mangold, N., Dromart, G., Ansan, V., Salese, F., Kleinhans, M. G., Massé, M., et al. (2020). Fluvial regimes, morphometry, and age of Jezero crater paleolake inlet valleys and their exobiological significance for the 2020 rover mission landing site. *Astrobiology*, *20*(8), 994–1013. https://doi.org/10.1089/ast.2019.2132

Mangold, N., Gupta, S., Gasnault, O., Dromart, G., Tarnas, J. D., Sholes, S. F., et al. (2021). Perseverance rover reveals an ancient delta-lake system and flood deposits at Jezero crater, Mars. *Science*, *374*(6568), 711–717. https://doi.org/10.1126/science.abl4051

Mangold, N., Poulet, F., Mustard, J. F., Bibring, J.-P., Gondet, B., Langevin, Y., et al. (2007). Mineralogy of the Nili Fossae region with OMEGA/Mars Express data: 2. Aqueous alteration of the crust. *Journal of Geophysical Research*, *112*(E8), E08S04. https://doi.org/10.1029/2006JE002835

Masursky, H. (1973). An overview of geological results from Mariner 9. *Journal of Geophysical Research*, *78*(20), 4009–4030. https://doi.org/10.1029/JB078i020p04009

McEwen, A. S., Eliason, E. M., Bergstrom, J. W., Bridges, N. T., Hansen, C. J., Delamere, W. A., et al. (2007). Mars reconnaissance orbiter's high resolution imaging science experiment (HiRISE). *Journal of Geophysical Research*, *112*(E5), E05S02. https://doi.org/10.1029/2005JE002605

McLennan, S. M., Sephton, M. A., Allen, C., Allwood, A. C., Barbieri, R., & Beaty, D. W. (2012). Planning for Mars returned sample science: Final report of the MSR end-to-end international science analysis group (E2E-iSAG). *Astrobiology*, *12*(3), 175–230. https://doi.org/10.1089/ast.2011.0805

Meyer-Peter, E., & Müller, R. (1948). Formulas for bed-load transport. In *Proceedings of the 2nd meeting of the international association for hydraulic structures research* (pp. 39–64). IAHR.

Mustard, J. F., Ehlmann, B. L., Murchie, S. L., Poulet, F., Mangold, N., Head, J. W., et al. (2009). Composition, morphology, and stratigraphy of Noachian crust around the Isidis basin. *Journal of Geophysical Research*, *114*(E2), E00D12. https://doi.org/10.1029/2009JE003349

Mustard, J. F., Poulet, F., Head, J. W., Mangold, N., Bibring, J.-P., Pelkey, S. M., et al. (2007). Mineralogy of Nili Fossae region with OMEGA/Mars express data: 1. Ancient impact melt in the Isidis basin and implications for the transition from the Noachian to Hesperian. *Journal of Geophysical Research*, *112*(E8), E08S03. https://doi.org/10.1029/2006JE002834

Pieri, D. C. (1980). Martian valleys: Morphology, distribution, age, and origin. *Science*, *210*(4472), 895–897. https://doi.org/10.1126/science.210.4472.895

Poulet, F., Bibring, J.-P., Mustard, J. F., Gendrin, A., Mangold, N., Langevin, Y., et al. (2005). Phyllosilicates on Mars and implications for early Martian climate. *Nature*, *438*(7068), 623–627. https://doi.org/10.1038/nature04274

Quantin-Nataf, C., Lozac'h, L., Thollot, P., Loizeau, D., Bultel, B., Fernando, J., et al. (2018). MarsSI: Martian surface data processing information system. *Planetary and Space Science*, *150*, 157–170. https://doi.org/10.1016/j.pss.2017.09.014

Salese, F., Kleinhans, M. G., Mangold, N., Ansan, V., McMahon, W., De Haas, T., & Dromart, G. (2020). Estimated minimum life span of the Jezero fluvial delta (Mars). *Astrobiology*, *20*(8), 977–993. https://doi.org/10.1089/ast.2020.2228

Salvatore, M. R., Goudge, T. A., Bramble, M. S., Edwards, C. S., Bandfield, J. L., Amador, E. S., et al. (2018). Bulk mineralogy of the NE Syrtis and Jezero crater regions of Mars derived through thermal infrared spectral analyses. *Icarus*, *301*, 76–96. https://doi.org/10.1016/j.icarus.2017.09.019

Schon, S. C., Head, J. W., & Fassett, C. I. (2012). An overfilled lacustrine system and progradational delta in Jezero crater, Mars: Implications for Noachian climate. *Planetary and Space Science*, *67*(1), 28–45. https://doi.org/10.1016/j.pss.2012.02.003

Schumm, S. A., & Ethridge, F. G. (1994). Origin, evolution and morphology of fluvial valleys. In R. W. Dalrymple, R. Boyd, & B. A. Zaitlin (Eds.), *Incised-valley systems: Origin and sedimentary sequences, SEPM society for sedimentary and geology* (Vol. 51, pp. 11–29). https://doi.org/10.2110/pec.94.12.0011

Sissons, J. B. (1961). A subglacial drainage system by the Tinto Hills, Lanarkshire. *Transactions of the Edinburgh Geological Society*, *18*(2), 175–193. https://doi.org/10.1144/transed.18.2.175

Spence, C., & Woo, M. K. (2003). Hydrology of subarctic Canadian shield: Soil-filled valleys. *Journal of Hydrology*, *279*(1–4), 151–166. https://doi.org/10.1016/S0022-1694(03)00175-6

Tarnas, J. D., Mustard, J. F., Lin, H., Goudge, T. A., Amador, E. S., Bramble, M. S., et al. (2019). Orbital identification of hydrated silica in Jezero crater, Mars. *Geophysical Research Letters*, *46*(22), 12771–12782. https://doi.org/10.1029/2019gl085584

Villette, J., Mangold, N., Kite, E., Conway, S., & Le Deit, L. (2025). Discharge and lake overflow models (Version 1) [Code]. *Zenodo*. https://doi.org/10.5281/zenodo.15183051

Volat, M., Quantin-Nataf, C., & Dehecq, A. (2022). Digital elevation model workflow improvements for the MarsSI platform and resulting orthorectified mosaic of Oxia Planum, the landing site of the ExoMars 2022 rover. *Planetary and Space Science*, *222*, 105552. https://doi.org/10.1016/j.pss.2022.105552

Walder, J., & Hallet, B. (1979). Geometry of former subglacial water channels and cavities. *Journal of Glaciology*, *23*(89), 335–346. https://doi.org/10.3189/S0022143000029944

Warner, N. H., Sowe, M., Gupta, S., Dumke, A., & Goddard, K. (2013). Fill and spill of giant lakes in the eastern Valles Marineris region of Mars. *Geology*, *41*(6), 675–678. https://doi.org/10.1130/G34172.1

Warren, A. O., Holo, S., Kite, E. S., & Wilson, S. A. (2021). Overspilling small craters on a dry Mars: Insights from breach erosion modeling. *Earth and Planetary Science Letters*, *554*, 116671. https://doi.org/10.1016/j.epsl.2020.116671

Wharton, R. A., Crosby, J. M., McKay, C. P., & Rice, J. W. (1995). Paleolakes on Mars. *Journal of Paleolimnology*, *13*, 267–283. https://doi.org/10.1007/BF00682769

Wilson, L., Ghatan, G. J., Head, J. W. III, & Mitchell, K. L. (2004). Mars outflow channels: A reappraisal of the estimation of water flow velocities from water depths, regional slopes and channel floor properties. *Journal of Geophysical Research*, *109*(E9), E09003. https://doi.org/10.1029/2004je002281

Zurek, R. W., & Smrekar, S. E. (2007). An overview of the Mars reconnaissance orbiter (MRO) science mission. *Journal of Geophysical Research*, *112*(E5), E05S01. https://doi.org/10.1029/2006JE002701